

An H^∞ /MinMax Periodic Control in a 2-D Structural Acoustic Model with Piezoceramic Actuators *

H. T. Banks[†] M. A. Demetriou[†] R. C. Smith[‡]

September 6, 1994

Abstract

A feedback control computational methodology for reducing acoustic sound pressure levels in a 2-D cavity with a flexible boundary (a beam) is investigated. The control is implemented in this model through voltages to piezoceramic patches on the beam which are excited in a manner (out-of-phase) so as to produce pure bending moments. The incorporation of the output feedback control in this system leads to a problem with unbounded input and output terms. By writing the resulting system as an abstract Cauchy equation, the problem of reducing interior pressure levels can be posed in the context of an H^∞ /MinMax time domain state space formulation. A summary of extensive computational efforts comparing output feedback with full state feedback and investigating the effect of the number and location of sensors on performance of the control is presented.

1 Introduction

In this paper we continue our earlier studies on the active control of a 2-D structural acoustic model through the use of piezoceramic actuators. The control methodology used here, unlike previous investigations, employs the recently developed H^∞ /MinMax formulation wherein a robust controller is designed to provide bounds on the effects of disturbances. Unlike our other studies where the full state is required for the implementation of a linear quadratic regulator (LQR) controller, we consider here controls based on the plant output, which may be corrupted by noise (measurement noise). The purpose of this paper is to report on several aspects of our investigations. First, we wished to study how the lack of full state output affects the performance of feedback controls derived using a standard LQR theory. In addition, we sought to test a methodology based on a robust formulation of the LQR theory - the so called H^∞ /MinMax approach - and to quantify, if possible,

*Research supported in part (H.T.B. and M.A.D.) by the Air Force Office of Scientific Research under grant AFOSR F49620-93-1-0198, and in part by NASA under grant NAG-1-1600. Research also supported in part by NASA under contracts NAS1-18605 and NAS1-19480 to ICASE while H.T.B. and R.C.S. were visiting scientists at ICASE, NASA Langley Research Center.

[†]Center for Research in Scientific Computation, North Carolina State University, Raleigh, NC 27695-8205

[‡]Department of Mathematics, Iowa State University, Ames, IA 50011

the effects of modeling/measurement noise and the location and number of sensors on the resulting control performance in our structural acoustics problem. We outline results of these investigations in the context of some of the same test examples studied in [2, 6] where a full state LQR feedback methodology was used.

In the next section we review the necessary background on the structure/acoustic interaction problem along with the mathematical formulae governing its dynamics. In Section 3, the problem is posed in a variational form. A Min-Max output feedback controller is introduced in Section 4 and an approximation scheme for this formulation is summarized in Section 5. Section 6 contains examples demonstrating both state and output feedback control results with some conclusions following in Section 7.

The 2-D structural acoustic model investigated in this paper represents a “linearized slice” of a full 3-D acoustic cavity/plate structure currently being used in experiments in the Acoustics Division at NASA Langley Research Center [7]. This 3-D apparatus consists of a concrete cylinder with a thin circular flexible plate at one end. Piezoceramic patches are mounted in pairs on the plate and can be used for both control of tangential and transverse vibrations and sensing of accumulated strain. Microphones are placed in the cylinder to provide acoustic pressure measurements. An exterior noise field excites the plate thus producing plate vibrations which in turn produce interior cavity noise. The cylinder walls and non-plate end of the cylinder are constructed from materials (concrete) so as to approximate a completely rigid structure for which hard wall boundary conditions are appropriate. If one “slices” the cylinder along its axis, one obtains the 2-D model depicted in Figure 1(a) wherein the plate becomes a flexible beam at one end of a 2-D cavity. Such 2-D models have been successfully used to study various questions related to identification and control methodologies for the 3-D structure ([2], [6], [8], [9]).

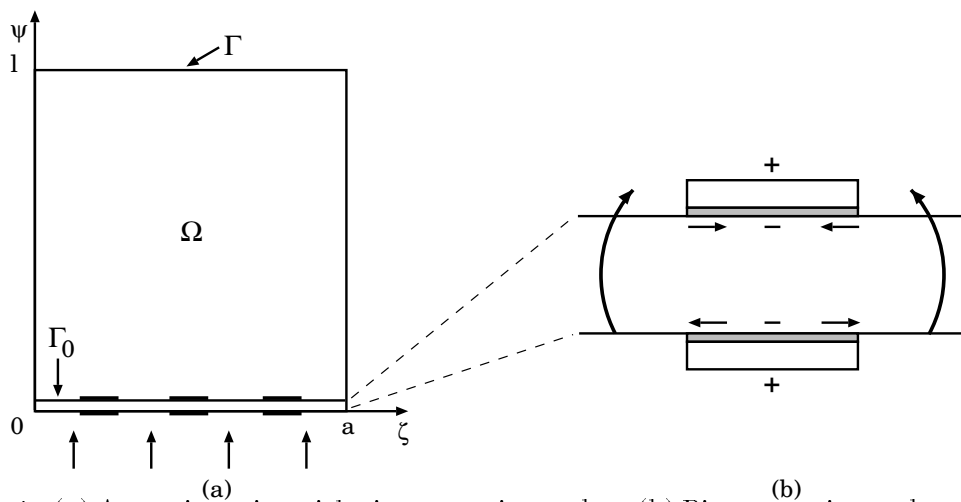


Figure 1: (a) Acoustic cavity with piezoceramic patches, (b) Piezoceramic patch excitation.

2 Mathematical Model

In developing control methodologies for acoustic wave motion in the fluid cavity $\Omega(t)$ of Figure 1(a), it is useful to introduce a velocity potential ϕ which is a real-valued function

satisfying $\vec{u}(t, \zeta, \psi) = -\nabla\phi(t, \zeta, \psi)$ where \vec{u} denotes the fluid's velocity. If the equilibrium density of the fluid is given by ρ_f , the acoustic pressure p is related to this velocity potential by $p(t, \zeta, \psi) = \rho_f\phi_t(t, \zeta, \psi)$. Under the usual assumptions [23] for acoustic waves with small amplitude, both the potential and the pressure satisfy the undamped first order wave equation with uniform speed of sound c in the fluid; hence we have

$$\phi_{tt} = c^2\Delta\phi \quad (\zeta, \psi) \in \Omega(t), \quad t > 0.$$

The boundary (denoted as Γ) on the three sides of the variable cavity $\Omega(t)$ are taken to be “hard” walls and thus the zero normal velocity conditions

$$\nabla\phi \cdot \hat{n} = 0 \quad (\zeta, \psi) \in \Gamma, \quad t > 0,$$

where \hat{n} is the outer normal, are appropriate. It furthermore is assumed that the perturbable boundary Γ_0 consists of an impenetrable fixed-end Euler-Bernoulli beam with Kelvin-Voigt damping. Letting $w(t, \zeta)$ denote the transverse displacement of the beam with linear mass density ρ_b , the equations of motion for the transverse vibrations of the beam are given by

$$\begin{aligned} \rho_b w_{tt} + \frac{\partial^2}{\partial \zeta^2} \mathcal{M}(t, \zeta) &= -\rho_f \phi_t(t, \zeta, w(t, \zeta)) + f(t, \zeta), \quad 0 < \zeta < a, \quad t > 0, \\ w(t, 0) = \frac{\partial w}{\partial \zeta}(t, 0) &= w(t, a) = \frac{\partial w}{\partial \zeta}(t, a) = 0, \quad t > 0. \end{aligned} \quad (2.1)$$

Here $\mathcal{M}(t, \zeta)$ is the total beam moment, $\rho_f \phi_t(t, \zeta, w(t, \zeta))$ is the backpressure due to the ensuing acoustic field inside the cavity, and f is the external applied force due to pressure from the exterior noise field. For a beam to which piezoceramic patches are bonded, the moment

$$\mathcal{M}(t, \zeta) = M(t, \zeta) - M_{pe}(t, \zeta)$$

consists of an internal component M , depending on material and geometric properties of the beam and patches, and an external component M_{pe} (the control term, see Figure 1(b)), which results from the activation of the patches through an applied voltage (see [2, 8, 9] for more detailed discussions).

For a beam undergoing pure bending motion with out-of-phase excitation of a single patch pair located in the interval $\alpha_1 \leq \zeta \leq \alpha_2$, the internal and external moments are given by

$$\begin{aligned} M(t, \zeta) &= EI(\zeta) \frac{\partial^2 w}{\partial \zeta^2} + c_D I(\zeta) \frac{\partial^3 w}{\partial \zeta^2 \partial t} \\ M_{pe}(t, \zeta) &= \mathcal{K}^B \chi_{[\alpha_1, \alpha_2]}(\zeta) u(t) \end{aligned} \quad (2.2)$$

where $u(t)$ is the voltage applied to the patches, $\chi_{[\alpha_1, \alpha_2]}(\zeta)$ is the characteristic function over the interval $[\alpha_1, \alpha_2]$ and \mathcal{K}^B is a parameter which depends on the geometry and piezoceramic material properties (e.g., see, [2, 8, 9]). Here EI and $c_D I$ are the stiffness and damping coefficients which, in physical examples, must be treated as varying in space due to the presence of the patches (see [10]). The final coupling equation in the beam-cavity system is the continuity of velocity condition

$$w_t(t, \zeta) = \nabla\phi(t, \zeta, w(t, \zeta)) \cdot \hat{n}, \quad 0 < \zeta < a, \quad t > 0, \quad (2.3)$$

which follows from the assumption that the beam is impenetrable to the fluid. Using the assumption of small displacements, (see [2] and [9]), the beam equation in (2.1) can be approximated by

$$\rho_b w_{tt} + \frac{\partial^2}{\partial \zeta^2} \mathcal{M}(t, \zeta) = -\rho_f \phi_t(t, \zeta, 0) + f(t, \zeta)$$

while (2.3) can be approximated by

$$w_t(t, \zeta) = \nabla \phi(t, \zeta, 0) \cdot \hat{n}.$$

By approximating (again under a small displacement assumption) the domain $\Omega(t)$ by the fixed domain $\Omega \equiv [0, a] \times [0, l]$, the approximate controlled model can be written as

$$\begin{aligned} \phi_{tt} &= c^2 \Delta \phi & (\zeta, \psi) \in \Omega, t > 0, \\ \nabla \phi \cdot \hat{n} &= 0 & (\zeta, \psi) \in \Gamma, t > 0, \\ \nabla \phi(t, \zeta, 0) \cdot \hat{n} &= w_t(t, \zeta) & 0 < \zeta < a, t > 0, \\ \rho_b w_{tt} + \frac{\partial^2}{\partial \zeta^2} \left(EI \frac{\partial^2 w}{\partial \zeta^2} + c_D I \frac{\partial^3 w}{\partial \zeta^2 \partial t} \right) &= -\rho_f \phi_t(t, \zeta, 0) \\ &+ f(t, \zeta) + \frac{\partial^2}{\partial \zeta^2} \left(\mathcal{K}^B \chi_{[\alpha_1, \alpha_2]} u(t) \right) & \begin{array}{l} 0 < \zeta < a, \\ t > 0, \end{array} \end{aligned} \quad (2.4)$$

$$w(t, 0) = \frac{\partial w}{\partial \zeta}(t, 0) = w(t, a) = \frac{\partial w}{\partial \zeta}(t, a) = 0 \quad t > 0,$$

$$\begin{aligned} \phi(0, \zeta, \psi) &= \phi_0(\zeta, \psi), & w(0, \zeta) &= w_0(\zeta) \\ \phi_t(0, \zeta, \psi) &= \phi_1(\zeta, \psi), & w_t(0, \zeta) &= w_1(\zeta). \end{aligned}$$

3 Abstract Formulation

To pose the system given in Section 2 in a first order abstract form which is convenient for feedback control and approximation, the state is taken to be $z = (\phi, w)$ in the state space $X = \overline{L}_2(\Omega) \times L_2(\Gamma_0)$ with the energy inner product

$$\left\langle \left(\begin{array}{c} \phi \\ w \end{array} \right), \left(\begin{array}{c} \xi \\ \lambda \end{array} \right) \right\rangle_X = \int_{\Omega} \frac{\rho_f}{c^2} \phi \xi d\omega + \int_{\Gamma_0} \rho_b w \lambda d\gamma.$$

Here $\overline{L}_2(\Omega)$ is the quotient space of L_2 over the constant functions. The quotient space is used since the velocity potentials are determined only up to a constant (e.g. see [2, 6]). We also define the Hilbert space $V = \overline{H}^1(\Omega) \times H_0^2(\Gamma_0)$ where $\overline{H}^1(\Omega)$ is the quotient space of $H^1(\Omega)$ over the constant functions and $H_0^2(\Gamma_0) = \{\varphi \in H^2(\Gamma_0) : \varphi(\zeta) = \varphi'(\zeta) = 0 \text{ at } \zeta = 0, a\}$. The V inner product is defined by

$$\left\langle \left(\begin{array}{c} \phi \\ w \end{array} \right), \left(\begin{array}{c} \xi \\ \lambda \end{array} \right) \right\rangle_V = \int_{\Omega} \nabla \phi \cdot \nabla \xi d\omega + \int_{\Gamma_0} D^2 w D^2 \lambda d\gamma.$$

Both X and V are Hilbert spaces with the inner products defined here being topologically equivalent to the standard product topologies for these spaces. Following the ideas in [2, 6] and letting V^* be the topological dual of V , we consider the Gelfand triple $V \hookrightarrow X \hookrightarrow V^*$ with pivot space X and define sesquilinear forms $\sigma_i : V \times V \rightarrow \mathbb{C}$, $i = 1, 2$ by

$$\begin{aligned}\sigma_1(\Phi, \Psi) &= \int_{\Omega} \rho_f \nabla \phi \cdot \nabla \xi d\omega + \int_{\Gamma_0} EID^2 w D^2 \lambda d\gamma \\ \sigma_2(\Phi, \Psi) &= \int_{\Gamma_0} \left\{ c_D ID^2 w D^2 \lambda + \rho_f (\phi \lambda - w \xi) \right\} d\gamma\end{aligned}$$

for all $\Phi = (\phi, w)$ and $\Psi = (\xi, \lambda)$ in V . If we now assume that the beam has s patch pairs attached at locations $[\alpha_{i1}, \alpha_{i2}]$, $i = 1, 2, \dots, s$, then we can write the input or control operator $B \in \mathcal{L}(U, V^*)$, with U denoting the Hilbert space containing the control inputs, as

$$\langle Bu, \Psi \rangle_{V^*, V} = \int_{\Gamma_0} \sum_{i=1}^s \mathcal{K}_i^B u_i \chi_{[\alpha_{i1}, \alpha_{i2}]} D^2 \lambda d\gamma,$$

for $\Psi \in V$. By setting $F = (0, f/\rho_b)$ we can write the control system (2.4) for the state $z(t) = (\phi(t), w(t)) \in V \subset X$ in variational form

$$\langle z_{tt}(t), \Psi \rangle_{V^*, V} + \sigma_2(z_t(t), \Psi) + \sigma_1(z(t), \Psi) = \langle Bu(t) + F, \Psi \rangle_{V^*, V} \quad \text{for all } \Psi \in V.$$

Adopting the ideas in [2, 3], we define the operators $A_i : V \rightarrow V^*$, $i = 1, 2$, by

$$\langle A_1 \Phi, \Psi \rangle_{V^*, V} = \sigma_1(\Phi, \Psi), \quad (3.1)$$

$$\langle A_2 \Phi, \Psi \rangle_{V^*, V} = \sigma_2(\Phi, \Psi), \quad (3.2)$$

for $\Phi = (\phi, w)$ and $\Psi = (\xi, \lambda)$ in V . The system in variational form can then be written as

$$\ddot{z}(t) + A_2 \dot{z}(t) + A_1 z(t) = Bu(t) + F(t) \quad \text{in } V^*.$$

Continuing with the abstract formulation, we may write the system in first order form. First define the product spaces $\mathcal{V} = V \times V$ and $\mathcal{X} = V \times X$ with the norms

$$|(\Phi, \Psi)|_{\mathcal{X}}^2 = |\Phi|_V^2 + |\Psi|_X^2 \quad \text{and} \quad |(\Phi, \Psi)|_{\mathcal{V}}^2 = |\Phi|_V^2 + |\Psi|_V^2.$$

It can then be shown (e.g. see [2, 3] for details) that we can define a system operator $\mathcal{A} : \mathcal{X} \rightarrow \mathcal{X}$ by

$$\mathcal{A} = \begin{bmatrix} 0 & I \\ -A_1 & -A_2 \end{bmatrix},$$

where $\mathcal{D}(\mathcal{A}) = \{\mu = (\Xi, \Lambda) \in \mathcal{X} : \Lambda \in V, A_1 \Xi + A_2 \Lambda \in X\}$, and A_1, A_2 are the operators defined above. We may then obtain a first order formulation given by

$$\dot{x}(t) = \mathcal{A}x(t) + \mathcal{B}u(t) + \mathcal{F}(t) \quad \text{in } \mathcal{V}^* \equiv V \times V^*, \quad (3.3)$$

where $x(t) = (z(t), \dot{z}(t))$, $\mathcal{F}(t) = (0, F(t))$, $\mathcal{B}u(t) = (0, Bu(t))$ and \mathcal{X} has been used as pivot space in defining $\mathcal{V} \subset \mathcal{X} \subset \mathcal{V}^*$ (see [2], [3], [6], [8] for details).

4 H^∞ /MinMax Periodic Control Problem

In this section we outline a methodology for an H^∞ /MinMax periodic control methodology for infinite dimensional systems. This can be viewed as a formal extension of finite dimensional results such as those found in [1]. Even though there is not yet a complete theory that include problems with all the features of the one under consideration here (i.e., second order weakly damped systems with unbounded input and output operators and periodic disturbances), there are a number of contributions related to other special cases, see [4], [11], [12], [13], [14], [15], [16], [17], [18], [19], [20], [21], [22], [24], [25]. Our current efforts on theoretical aspects of the theory presented here will be presented elsewhere.

We consider the system (in the form given in the previous section) with a periodic external force $\mathcal{F}(t)$ with period τ and an added disturbance (error) input denoted by $\eta(t)$, thus giving

$$\dot{x}(t) = \mathcal{A}x(t) + \mathcal{B}u(t) + \mathcal{D}\eta(t) + \mathcal{F}(t), \quad (4.1)$$

with $x(0) = x(\tau)$. The performance output $z(t) \in Z$ is given by

$$z(t) = \mathcal{H}x(t) + \mathcal{G}u(t), \quad (4.2)$$

where Z is a performance output space and $\mathcal{H} : \mathcal{X} \rightarrow Z$, $\mathcal{G} : U \rightarrow Z$. The disturbance evolves in a space \mathcal{W} and it is assumed that $\mathcal{D} : \mathcal{W} \rightarrow \mathcal{X}$ with $\mathcal{H}^*\mathcal{G} = 0$. The general control problem can then be formulated as the problem of finding $u \in L_2(0, \tau; U)$ which minimizes the steady-state disturbance-augmented functional (or, equivalently, the ‘‘soft-constrained’’ disturbance attenuation index)

$$J(u) = \int_0^\tau \left\{ \langle \mathcal{Q}x(t), x(t) \rangle_{\mathcal{X}} + \langle Ru(t), u(t) \rangle_U - \gamma^2 |\eta(t)|_{\mathcal{W}}^2 \right\}, \quad (4.3)$$

where $\mathcal{Q} \equiv \mathcal{H}^*\mathcal{H}$ and $R \equiv \mathcal{G}^*\mathcal{G}$. Here $\gamma \in \mathcal{R}$ is a fixed positive constant which is a design parameter to be chosen as small as possible while the corresponding control law produces an exponentially stable closed-loop system. In this case, the H^∞ norm of the closed loop disturbance to performance output transfer function from $\eta(\cdot)$ to $z(\cdot)$ is bounded above by γ . The operator \mathcal{Q} is chosen so as to emphasize the minimization of particular state variables (see [2, 6]). The control space U is taken to be \mathbb{R}^s if s patches are used in the model, and it is assumed that the operator $R = \text{diag}(r_{ii})$ is an $s \times s$ diagonal matrix where $r_{ii} > 0$, $i = 1, \dots, s$ is the weight on the controlling voltage into the i^{th} patch.

If it is assumed that the state $x(t)$ is available, then under certain stabilizability and detectability assumptions on the system and standard assumptions on \mathcal{Q} , the optimal control is given by

$$u(t) = -R^{-1}\mathcal{B}^*[\Pi x(t) - r(t)]. \quad (4.4)$$

Here $\Pi \in \mathcal{L}(\mathcal{V}^*, \mathcal{V})$ is the unique nonnegative self adjoint solution to the algebraic operator Riccati equation

$$\Pi\mathcal{A} + \mathcal{A}^*\Pi - \Pi \left(\mathcal{B}R^{-1}\mathcal{B}^* - \frac{1}{\gamma^2}\mathcal{D}\mathcal{D}^* \right) \Pi + \mathcal{Q} = 0, \quad (4.5)$$

$r(t)$ is the unique τ -periodic solution of

$$\dot{r}(t) + \left[\mathcal{A} - \left(\mathcal{B}R^{-1}\mathcal{B}^*\Pi - \frac{1}{\gamma^2}\mathcal{D}\mathcal{D}^*\Pi \right) \right]^* r(t) - \Pi\mathcal{F}(t) = 0, \quad (4.6)$$

and the resulting optimal trajectory x is the solution of

$$\dot{x}(t) = \left[\mathcal{A} - \mathcal{B}R^{-1}\mathcal{B}^*\Pi \right] x(t) + \mathcal{B}R^{-1}\mathcal{B}^*r(t) + \mathcal{D}\eta(t) + \mathcal{F}(t). \quad (4.7)$$

Under appropriate assumptions, see [4] and [12], one finds that both operators

$$\mathcal{A} - \mathcal{B}R^{-1}\mathcal{B}^*\Pi, \quad \text{and} \quad \mathcal{A} - \left(\mathcal{B}R^{-1}\mathcal{B}^* - \frac{1}{\gamma^2}\mathcal{D}\mathcal{D}^* \right) \Pi,$$

generate exponentially stable \mathcal{C}_0 semigroups on \mathcal{X} which are then extended through extrapolation space techniques to a larger space which contains the control input and forcing terms, see [5].

In general, however, one seldom has the full state x available for measurement and control implementation. Instead, only a measured output $y \in Y$ given by

$$y(t) = \mathcal{C}x(t) + \mathcal{E}\eta(t), \quad (4.8)$$

is available, where Y denotes the output space and $\mathcal{C} : \mathcal{X} \rightarrow Y$, $\mathcal{E} : \mathcal{W} \rightarrow Y$. It is assumed here that $\mathcal{E}\mathcal{E}^* \equiv \mathcal{N}$ with \mathcal{N} invertible and $\mathcal{D}\mathcal{E}^* = 0$. In order to satisfy the condition $\mathcal{D}\mathcal{E}^* = 0$ which would maintain a certain symmetry, [1], and guarantee that the disturbance signal for the state (entering through the operator \mathcal{D}) and the disturbance signal for the output (entering through the operator \mathcal{E}) be independent, we could have chosen

$$\tilde{\mathcal{D}} = [\mathcal{D} \ 0] \quad \text{and} \quad \tilde{\mathcal{E}} = [0 \ \mathcal{E}],$$

which essentially gives $\tilde{\mathcal{D}}\tilde{\mathcal{E}}^* = 0$. Instead, for implementational ease (which effectively simplifies the numerical implementation of the scheme), we considered the case where the term $\mathcal{D}\eta(t)$ in (4.7) is given by $\mathcal{D}\eta_1(t)$ and the term $\mathcal{E}\eta(t)$ in (4.8) is given by $\mathcal{E}\eta_2(t)$, with $\eta_1(t)$ and $\eta_2(t)$ independent.

Hence, this output must be used to construct a compensator or state estimator. The equation of the state estimator is given by

$$\begin{aligned} \dot{\hat{x}}(t) &= \left[\mathcal{A} - \left(\mathcal{B}R^{-1}\mathcal{B}^* - \frac{1}{\gamma^2}\mathcal{D}\mathcal{D}^* \right) \Pi \right] \hat{x}(t) + \left[\mathcal{B}R^{-1}\mathcal{B}^* - \frac{1}{\gamma^2}\mathcal{D}\mathcal{D}^* \right] r(t) \\ &+ \mathcal{F}(t) + \left(I - \frac{1}{\gamma^2}\Sigma\Pi \right)^{-1} \Sigma\mathcal{C}^*\mathcal{N}^{-1} (y(t) - \mathcal{C}\hat{x}(t)), \end{aligned} \quad (4.9)$$

and the optimal control is then

$$u(t) = -R^{-1}\mathcal{B}^* [\Pi\hat{x}(t) - r(t)]. \quad (4.10)$$

The tracking variable $r(t)$ is the unique τ -periodic solution of

$$\dot{r}(t) + \left[\mathcal{A} - \left(\mathcal{B}R^{-1}\mathcal{B}^*\Pi - \frac{1}{\gamma^2}\mathcal{D}\mathcal{D}^*\Pi \right) \right]^* r(t) - \Pi\mathcal{F}(t) = 0, \quad (4.11)$$

which is identical to equation (4.6). The unique self adjoint operators, Π and Σ satisfy the following control and observer algebraic Riccati equations,

$$\Pi\mathcal{A} + \mathcal{A}^*\Pi - \Pi \left(\mathcal{B}R^{-1}\mathcal{B}^* - \frac{1}{\gamma^2}\mathcal{D}\mathcal{D}^* \right) \Pi + \mathcal{Q} = 0, \quad (4.12)$$

$$\Sigma \mathcal{A}^* + \mathcal{A} \Sigma - \Sigma \left(\mathcal{C}^* \mathcal{N}^{-1} \mathcal{C} - \frac{1}{\gamma^2} \mathcal{Q} \right) \Sigma + \mathcal{D} \mathcal{D}^* = 0. \quad (4.13)$$

In addition to self adjointness of the operators Π and Σ , we also impose the condition that $\Sigma(I - \frac{1}{\gamma^2} \Pi \Sigma)^{-1} \in \mathcal{L}(\mathcal{V}^*, \mathcal{V})$ is coercive or equivalently that $(I - \frac{1}{\gamma^2} \Pi \Sigma)$ is invertible (see [1, 12, 16]). This also translates to the boundedness of the spectral radius of $\Sigma \Pi$ by γ^2 which is known as the coupling equation defined in [16] (also known as the γ^2 robustness property as defined in [12])

$$r_{sp}(\Sigma \Pi) < \gamma^2. \quad (4.14)$$

For our simulation studies of the above problem, it was assumed that a number of displacement (n_{displ}) and velocity (n_{vel}), sensors placed at points ζ_i , $i = 1, \dots, n_{displ}$ or n_{vel} , are available to measure the displacement and velocity of the beam, and a number of microphones (n_{mic}) placed inside the cavity at points (ζ_i, ψ_i) , $i = 1, \dots, n_{mic}$, can measure the cavity pressure at certain locations. The disturbance entering the measured output, $\mathcal{E} \eta_2(t)$, was taken to be the largest amplitude of the open loop (i.e., $u(t) = 0$) output, for each individual sensor/microphone multiplied by a percentage (denoted as the % disturbance level in the results reported below) of a random (uniformly distributed) number in $[0, 1]$. Similarly, the modeling disturbance, $\mathcal{D} \eta_1(t)$, was taken to be the largest amplitude occurring in the time interval $[t_0, t_f]$ of interest of each individual component of the vector $x(t)$ in the open loop case multiplied by a percentage of a uniformly distributed random number on $[0, 1]$ which is independent of the random number in the measured output. Therefore, the output is given by

$$y(t) = \begin{bmatrix} w(t, \zeta_i) + w_i \alpha_2(t) \\ \rho_f \phi_t(t, \zeta_i, \psi_i) + p_i \alpha_2(t) \\ w_t(t, \zeta_i) + v_i \alpha_2(t), \end{bmatrix}, \quad (4.15)$$

where $\alpha_2(t)$ is a random number on $[0, 1]$ with uniform distribution and the weights w_i , $i = 1, \dots, n_{displ}$, v_j , $j = 1, \dots, n_{vel}$, and p_k , $k = 1, \dots, n_{mic}$ are given by

$$\begin{cases} w_i = \max_{t \in [t_0, t_f]} \{w(t, \zeta_i)_{OL}\}, & i = 1, \dots, n_{displ} \\ p_k = \max_{t \in [t_0, t_f]} \{\rho_f \phi_t(t, \zeta_k, \psi_k)_{OL}\}, & k = 1, \dots, n_{mic} \\ v_j = \max_{t \in [t_0, t_f]} \{w_t(t, \zeta_j)_{OL}\}, & j = 1, \dots, n_{vel} \end{cases} \quad (4.16)$$

Similarly, for $\Psi = (\xi, \lambda)$ the operator \mathcal{D} is given by

$$\mathcal{D} \eta_1(t) = \begin{bmatrix} \left(\int_{\Omega} 1.0 \cdot \nabla \xi d\omega \right) \cdot \eta_{1\phi}(t) \\ \left(\int_{\Gamma_0} 1.0 \cdot D^2 \lambda d\gamma \right) \cdot \eta_{1w}(t) \\ \left(\frac{\rho_f}{c^2} \int_{\Omega} 1.0 \cdot \xi d\omega \right) \cdot \eta_{1\phi_t}(t) \\ \left(\rho_b \int_{\Gamma_0} 1.0 \cdot \lambda d\gamma \right) \cdot \eta_{1w_t}(t) \end{bmatrix}, \quad (4.17)$$

where

$$\eta_{1\phi}(t) = 0.0$$

$$\eta_{1w}(t) = 0.0$$

$$\eta_{1\dot{\phi}}(t) = \max_{t \in [t_0, t_f]} \{ \phi_{tt}(t, \zeta, \psi)_{OL} \} \cdot \alpha_1(t),$$

$$\eta_{1\dot{w}}(t) = \max_{t \in [t_0, t_f]} \{ w_{tt}(t, \zeta)_{OL} \} \cdot \alpha_1(t),$$

with $\alpha_1(t)$ a random number (independent of $\alpha_2(t)$) with uniform distribution on $[0, 1]$. We point out that each component of $\mathcal{D}\eta_1(t)$ is the (X or V) inner product of 1 with the four components ϕ , w , $\dot{\phi}_t$ and w_t . This essentially results in a spatial distribution of the disturbance. This seems to be the most general modeling of the disturbance influence on the state $x(t)$ and output $y(t)$. In the results reported below, we comment on the effects of this weighting on the numerical solutions of (4.12) - (4.13).

5 Finite Dimensional Approximation

The state space approach presented in the previous section facilitates approximation techniques required for implementing the control laws. Due to the infinite dimensionality of the system given by (4.4) - (4.7) and/or (4.9) - (4.13), the approximation technique is required to obtain the approximate feedback gains. In the work reported here, we followed the approach in [2], [6], [8], using a Galerkin approximation scheme to approximate the beam/cavity system. This was achieved by discretizing the potential and beam terms in terms of spectral and spline expansions, respectively.

Our scheme for the first order formulation approximating (3.3) was of dimension $2N$ where $N = m + n - 1$ with $n - 1$ modified cubic splines used for the beam approximation and m tensor products of Legendre polynomials used for the cavity approximation (see [2] for complete details).

5.1 Finite Dimensional System

Using a standard Galerkin scheme, we choose a sequence of finite dimensional subspaces $\mathcal{X}^N \subset \mathcal{X}$ with projections $\mathcal{P}^N : \mathcal{X} \rightarrow \mathcal{X}^N$. The approximating problem in \mathcal{X}^N becomes the problem of finding $u \in L_2(0, \tau; U)$ which minimizes the “soft constrained” minimization index

$$J^N(u) = \int_0^\tau \left\{ \langle \mathcal{Q}x^N(t), x^N(t) \rangle_{\mathcal{X}} + \langle Ru(t), u(t) \rangle_U - \gamma^2 |\eta(t)|_{\mathcal{W}}^2 \right\} dt \quad (5.1)$$

subject to an approximating system

$$\begin{aligned} \dot{x}^N(t) &= \mathcal{A}^N x^N(t) + \mathcal{B}^N u(t) + \mathcal{D}^N \eta_1(t) + \mathcal{F}^N(t), \\ x^N(0) &= x^N(\tau) = \mathcal{P}^N x(0), \\ y^N(t) &= \mathcal{C}^N x^N(t) + \mathcal{E}^N \eta_2(t), \end{aligned}$$

where $(\cdot)^N$ denote the finite dimensional representations of the corresponding operators presented in Sections 3 and 4 above. The optimal approximate control is given by

$$u^N(t) = -R^{-1} \mathcal{B}^{N*} \left[\Pi^N \hat{x}^N(t) - r^N(t) \right],$$

with the finite dimensional representation of (4.3) given by

$$\dot{x}^N(t) = \mathcal{A}^N x^N(t) - \mathcal{B}^N R^{-1} \mathcal{B}^{N*} \Pi^N \hat{x}^N(t) + \mathcal{B} R^{-1} \mathcal{B}^{N*} r^N(t) + \mathcal{D}^N \eta_1(t) + \mathcal{F}^N(t),$$

and that of (4.9) given by

$$\begin{aligned} \dot{\hat{x}}^N(t) &= \left[\mathcal{A}^N - \left(\mathcal{B}^N R^{-1} \mathcal{B}^{N*} - \frac{1}{\gamma^2} \mathcal{D}^N \mathcal{D}^{N*} \right) \Pi^N \right] \hat{x}^N(t) \\ &+ \left[\mathcal{B}^N R^{-1} \mathcal{B}^{N*} - \frac{1}{\gamma^2} \mathcal{D}^N \mathcal{D}^{N*} \right] r^N(t) + \mathcal{F}^N(t) \\ &+ \left(I - \frac{1}{\gamma^2} \Sigma^N \Pi^N \right)^{-1} \Sigma^N \mathcal{C}^{N*} (\mathcal{N}^N)^{-1} \left(y^N(t) - \mathcal{C}^N \hat{x}^N(t) \right). \end{aligned}$$

Here Π^N and Σ^N are the finite dimensional representations of Π and Σ , respectively, and are the unique nonnegative self-adjoint solutions of

$$\begin{aligned} \Pi^N \mathcal{A}^N + \mathcal{A}^{N*} \Pi^N - \Pi^N \left(\mathcal{B}^N R^{-1} \mathcal{B}^{N*} - \frac{1}{\gamma^2} \mathcal{D}^N \mathcal{D}^{N*} \right) \Pi^N + \mathcal{Q}^N &= 0, \\ \Sigma^N \mathcal{A}^{N*} + \mathcal{A}^N \Sigma^N - \Sigma^N \left(\mathcal{C}^{N*} (\mathcal{N}^N)^{-1} \mathcal{C}^N - \frac{1}{\gamma^2} \mathcal{Q}^N \right) \Sigma^N + \mathcal{D}^N \mathcal{D}^{N*} &= 0. \end{aligned}$$

Also, $r^N(t)$ is the approximation of $r(t)$ in (4.11) and is the unique τ -periodic solution of

$$\dot{r}^N(t) + \left[\mathcal{A}^N - \left(\mathcal{B}^N R^{-1} \mathcal{B}^{N*} \Pi^N - \frac{1}{\gamma^2} \mathcal{D}^N \mathcal{D}^{N*} \Pi^N \right) \right]^* r^N(t) - \Pi^N \mathcal{F}^N(t) = 0.$$

5.2 Approximation Scheme

To illustrate the approximation technique mentioned above we let $\{B_i^n\}_{i=1}^{n-1}$ denote the 1-D cubic spline basis functions which are used to discretize the beam and let $\{B_i^m\}_{i=1}^m$, $m = (m_\xi + 1) \cdot (m_\psi + 1) - 1$, denote the 2-D Legendre basis functions which are used in the cavity. The $n - 1$ and m dimensional approximating subspaces are then taken to be $H_b^n = \text{span}\{B_i^n\}_{i=1}^{n-1}$ and $H_c^m = \{B_i^m\}_{i=1}^m$, respectively. Defining $N = m + n - 1$, the approximating state space is $X^N = H_c^m \times H_b^n$ and the product space for the first order system is $\mathcal{X}^N = X^N \times X^N$. The finite-dimensional approximation is then determined by restricting σ to $\mathcal{X}^N \times \mathcal{X}^N$. This yields the operator $\mathcal{A}^N : \mathcal{X}^N \rightarrow \mathcal{X}^N$ where

$$\mathcal{A}^N = \begin{bmatrix} 0 & I \\ -A_1^N & -A_2^N \end{bmatrix}$$

and A_1^N and A_2^N are obtained by restricting σ_1 and σ_2 to $X^N \times X^N$, [2]. The restriction of the infinite dimensional system to the space $\mathcal{X}^N \times \mathcal{X}^N$ yields for $\Psi = (\xi, \lambda)$ the system

$$\begin{aligned} \langle z_{tt}^N(t), \Psi \rangle_X &+ \sigma_2(z_t^N(t), \Psi) + \sigma_1(z^N(t), \Psi) \\ &= \int_{\Gamma_0} \mathcal{K}^B u(t) (H_{11} - H_{12}) D^2 \lambda d\gamma + \int_{\Gamma_0} f \lambda d\gamma \\ &+ \left\{ \int_{\Omega} 1 \cdot \nabla \xi d\omega + \int_{\Gamma_0} 1 \cdot D^2 \lambda d\gamma + \frac{\rho_f}{c^2} \int_{\Omega} 1 \cdot \xi d\omega + \rho_b \int_{\Gamma_0} 1 \cdot \lambda d\gamma \right\} \eta_1(t). \end{aligned}$$

When Ψ is chosen in X^N and the approximate beam and cavity solutions are taken to be

$$w^N(t, \zeta) = \sum_{i=1}^{n-1} w_i^N(t) B_i^n(\zeta) \quad \text{and} \quad \phi^N(t, \zeta, \psi) = \sum_{i=1}^m \phi_i^N(t) B_i^m(\zeta, \psi),$$

respectively, this yields the system

$$\begin{aligned} M^N \dot{z}^N(t) &= \tilde{A}^N z^N(t) + \tilde{B}^N u(t) + \tilde{D}^N \eta_1(t) + \tilde{F}^N(t), \\ M^N z^N(0) &= \tilde{z}_0^N, \\ y^N(t) &= C^N z^N(t) + E^N \eta_2(t), \end{aligned}$$

where

$$z^N(t) = \begin{pmatrix} \vartheta^N(t) \\ \dot{\vartheta}^N(t) \end{pmatrix}.$$

Here

$$\vartheta^N(t) = \begin{bmatrix} \phi_1^N(t) \\ \vdots \\ \phi_m^N(t) \\ w_1^N(t) \\ \vdots \\ w_{n-1}^N(t) \end{bmatrix},$$

contains the $N \times 1 = (m + n - 1) \times 1$ approximate state vector coefficients. The full system has the form

$$\begin{aligned} \begin{bmatrix} M_1^N & \mathbf{0} \\ \mathbf{0} & M_2^N \end{bmatrix} \begin{bmatrix} \dot{\vartheta}^N(t) \\ \ddot{\vartheta}^N(t) \end{bmatrix} &= \begin{bmatrix} \mathbf{0} & M_1^N \\ -A_1^N & -A_2^N \end{bmatrix} \begin{bmatrix} \vartheta^N(t) \\ \dot{\vartheta}^N(t) \end{bmatrix} + \begin{bmatrix} \mathbf{0} \\ \tilde{B}^N \end{bmatrix} u(t) \\ &+ \begin{bmatrix} \tilde{D}_1^N \\ \tilde{D}_2^N \end{bmatrix} \eta_1(t) + \begin{bmatrix} \mathbf{0} \\ \tilde{F}^N(t) \end{bmatrix}, \end{aligned}$$

$$y^N(t) = C^N \begin{bmatrix} \vartheta^N(t) \\ \dot{\vartheta}^N(t) \end{bmatrix} + E^N \eta_2(t),$$

$$\begin{bmatrix} M_1^N & \mathbf{0} \\ \mathbf{0} & M_2^N \end{bmatrix} \begin{bmatrix} \vartheta^N(0) \\ \dot{\vartheta}^N(0) \end{bmatrix} = \begin{bmatrix} g_1^N \\ g_2^N \end{bmatrix},$$

with

$$M_1^N = \text{diag}[M_{11}^N, M_{12}^N], \quad M_2^N = \text{diag}[M_{21}^N, M_{22}^N],$$

$$A_1^N = \text{diag}[A_{11}^N, A_{12}^N], \quad A_2^N = \begin{bmatrix} \mathbf{0} & A_{31}^N \\ A_{32}^N & A_{22}^N \end{bmatrix},$$

and

$$\tilde{B}^N = \begin{bmatrix} 0 \\ \tilde{B}_2^N \end{bmatrix}, \quad \tilde{F}^N = \begin{bmatrix} 0 \\ \tilde{F}_2^N(t) \end{bmatrix}.$$

For this specific system, the term $\tilde{D}^N \eta_1(t)$ is given by

$$\begin{aligned} \tilde{D}^N \eta_1(t) &= \begin{bmatrix} \tilde{D}_1^N & 0 \\ 0 & \tilde{D}_2^N \end{bmatrix} \cdot \eta_1(t) = \begin{bmatrix} [\tilde{D}_{11}^N]_l & 0 & 0 & 0 \\ 0 & [\tilde{D}_{12}^N]_p & 0 & 0 \\ 0 & 0 & [\tilde{D}_{21}^N]_l & 0 \\ 0 & 0 & 0 & [\tilde{D}_{22}^N]_p \end{bmatrix} \cdot \eta_1(t) \\ &= \begin{bmatrix} (\int_{\Omega} 1.0 \cdot \nabla B_l^m d\omega) \cdot \eta_{1\phi^N}(t), & l = 1, \dots, m, \\ (\int_{\Gamma_0} 1.0 \cdot D^2 B_p^n d\gamma) \cdot \eta_{1w^N}, & p = 1, \dots, n-1, \\ (\frac{\rho f}{c^2} \int_{\Omega} 1.0 \cdot B_l^m d\omega) \cdot \eta_{1\phi_t^N}(t), & l = 1, \dots, m, \\ (\rho b \int_{\Gamma_0} 1.0 \cdot B_p^n d\gamma) \cdot \eta_{1w_t^N}(t), & p = 1, \dots, n-1, \end{bmatrix}, \end{aligned}$$

where

$$\eta_{1\phi^N}(t) = 0,$$

$$\eta_{1w^N}(t) = 0,$$

$$\eta_{1\phi_t^N}(t) = \frac{\max_{t \in [t_0, t_f]} \{\phi_{it}^N(t, \zeta, \psi)_{OL}\}}{\max\{[(M_{21})^{-1} \tilde{D}_{21}^N]\}} \cdot \alpha_1(t),$$

$$\eta_{1w_t^N}(t) = \frac{\max_{t \in [t_0, t_f]} \{w_{it}^N(t, \zeta)_{OL}\}}{\max\{[(M_{22})^{-1} \tilde{D}_{22}^N]\}} \cdot \alpha_1(t).$$

If it is assumed that m_{out} outputs are used, then the $m_{out} \times N$ matrix C^N is given by

$$C^N \begin{bmatrix} \phi^N(t) \\ w^N(t) \\ \dot{\phi}_t^N(t) \\ \dot{w}_t^N(t) \end{bmatrix} = \begin{bmatrix} [0] & 0 & 0 & 0 \\ 0 & [C_{displ}] & 0 & 0 \\ 0 & 0 & [C_{press}] & 0 \\ 0 & 0 & 0 & [C_{vel}] \end{bmatrix} \begin{bmatrix} \phi^N(t) \\ w^N(t) \\ \phi_t^N(t) \\ w_t^N(t) \end{bmatrix},$$

with

$$[C_{displ}] = [C_{displ}^{i_d}]_{i_d} = \left[\int_{\Gamma_0} \delta(\zeta - \zeta_{i_d}) B_{k_d}^n(\zeta) d\zeta \right]_{i_d} = [B_{k_d}^n(\zeta_{i_d})],$$

$$[C_{press}] = [C_{press}^{i_p}]_{i_p} = \left[\rho f \int_{\Omega} \delta(\zeta - \zeta_{i_p}, \psi - \psi_{i_p}) B_{k_p}^m(\zeta, \psi) d\omega \right]_{i_p} = [\rho f B_{k_p}^m(\zeta_{i_p}, \psi_{i_p})],$$

$$[C_{vel}] = [C_{vel}^{i_v}]_{i_v} = \left[\int_{\Gamma_0} \delta(\zeta - \zeta_{i_v}) B_{k_v}^n(\zeta) d\zeta \right] = [B_{k_v}^n(\zeta_{i_v})],$$

where $\delta(\zeta - \zeta_i)$ and $\delta(\zeta - \zeta_i, \psi - \psi_i)$ are the one and two dimensional Dirac delta functions, respectively, and $k_d = 1, \dots, n-1$, $i_d = 1, \dots, n_{displ}$, $k_p = 1, \dots, m$, $i_p = 1, \dots, n_{mic}$, $k_v = 1, \dots, n-1$, $i_v = 1, \dots, n_{vel}$. The $m_{out} \times m_{out}$ matrix E^N is given by

$$E^N \eta_2(t) = \begin{bmatrix} 1 & 0 & \cdots & 0 & 0 \\ 0 & 1 & \cdots & 0 & 0 \\ \vdots & \vdots & \ddots & \vdots & \vdots \\ 0 & 0 & \cdots & 1 & 0 \\ 0 & 0 & \cdots & 0 & 1 \end{bmatrix} \left(\begin{bmatrix} e_1 \\ e_2 \\ \vdots \\ e_{m_{out}-1} \\ e_{m_{out}} \end{bmatrix} \alpha_2(t) \right) = \begin{bmatrix} \max_t \{w(t, \zeta_1)_{OL}\} \\ \vdots \\ \max_t \{w(t, \zeta_{n_{displ}})_{OL}\} \\ \max_t \{\rho_f \phi_t(t, \zeta_1, \psi_1)_{OL}\} \\ \vdots \\ \max_t \{\rho_f \phi_t(t, \zeta_{n_{mic}}, \psi_{n_{mic}})_{OL}\} \\ \max_t \{w_t(t, \zeta_1)_{OL}\} \\ \vdots \\ \max_t \{w_t(t, \zeta_{n_{vel}})_{OL}\} \end{bmatrix} \alpha_2(t)$$

where $\alpha_2(t)$ is a random number with uniform distribution on $[0, 1]$. The initial conditions given by the vectors $g_1^N = [g_{11}^N, g_{12}^N]$ and $g_2^N = [g_{21}^N, g_{22}^N]$ have elements

$$g_{11}^N = \int_{\Omega} \nabla \phi_0 \cdot \nabla B_l^m d\omega, \quad g_{12}^N = \int_{\Gamma_0} D^2 w_0 \cdot D^2 B_p^n d\gamma, \\ g_{21}^N = \frac{\rho_f}{c^2} \int_{\Omega} \phi_1 \cdot B_l^m d\omega, \quad g_{22}^N = \rho_b \int_{\Gamma_0} w_1 \cdot B_p^n d\gamma,$$

The system can now be written as a set of $2N$ ordinary differential equations given by

$$\dot{z}(t)^N = A^N z^N(t) - B^N R^{-1} (B^N)^T \Pi^N \hat{z}^N(t) + B^N R^{-1} (B^N)^T r^N(t) + D^N \eta_1(t) + F^N(t)$$

$$\begin{aligned} \dot{\hat{z}}^N(t) &= \left[A^N - \left(B^N R^{-1} (B^N)^T - \frac{1}{\gamma^2} D^N (D^N)^T \right) \Pi^N \right] \hat{z}^N(t) \\ &+ \left[B^N R^{-1} (B^N)^T - \frac{1}{\gamma^2} D^N (D^N)^T \right] r^N(t) + F^N(t) \\ &+ \left(I - \frac{1}{\gamma^2} \Sigma^N \Pi^N \right)^{-1} \Sigma^N (C^N)^T (\mathcal{N}^N)^{-1} (y^N(t) - C^N z^N(t)) \end{aligned}$$

with initial conditions

$$z^N(0) = z_0^N = z^N(\tau), \quad \hat{z}^N(0) = \hat{z}_0^N = \hat{z}^N(\tau) \neq z_0^N,$$

where $A^N = (M^N)^{-1} \tilde{A}^N$, $B^N = (M^N)^{-1} \tilde{B}^N$, $D^N = (M^N)^{-1} \tilde{D}^N$, $F^N = (M^N)^{-1} \tilde{F}^N$, $z_0^N = (M^N)^{-1} \tilde{z}_0^N$, and $\hat{z}_0^N = (M^N)^{-1} \tilde{\hat{z}}_0^N$. The matrices Π^N and Σ^N are solutions to the following algebraic matrix Riccati equations

$$\begin{aligned} \Pi^N A^N + (A^N)^T \Pi^N - \Pi^N \left(B^N R^{-1} (B^N)^T - \frac{1}{\gamma^2} D^N (D^N)^T \right) \Pi^N + Q^N &= 0, \\ \Sigma^N (A^N)^T + A^N \Sigma^N - \Sigma^N \left((C^N)^T (\mathcal{N}^N)^{-1} C^N - \frac{1}{\gamma^2} Q^N \right) \Sigma^N + D^N (D^N)^T &= 0, \end{aligned} \tag{5.2}$$

that also satisfy the coupling equation

$$r_{sp} \left(\Sigma^N \Pi^N \right) < \gamma^2.$$

Since Q^N denotes the matrix representation for the operator \mathcal{Q}^N , a suitable choice for Q^N is

$$Q^N = \Delta \begin{bmatrix} M_1^N & 0 \\ 0 & M_2^N \end{bmatrix},$$

where the diagonal matrix Δ is given by

$$\Delta = \text{diag} [d_1 I^m, d_2 I^{n-1}, d_3 I^m, d_4 I^{n-1}].$$

As it was pointed out in [2, 8], with the above choice for Q^N , the first inner product in the definition of $J^N(u)$ simplifies to

$$\begin{aligned} \langle Q^N z^N(t), z^N(t) \rangle_{\mathcal{X}^N} &= d_1 \int_{\Omega} |\nabla \phi^N|^2 d\omega + d_2 \int_{\Gamma_0} (D^2 w^N)^2 d\gamma \\ &+ d_3 \int_{\Omega} \frac{\rho_f}{c^2} (\dot{\phi}^N)^2 d\omega + d_4 \int_{\Gamma_0} \rho_b (\dot{w}^N)^2 d\gamma. \end{aligned}$$

This in essence minimizes the finite dimensional approximations to the kinetic and potential energies of the undamped beam and wave equation, [2].

For the regulator/compensator problem with periodic forcing function $F^N(t)$, $r^N(t)$ solves the linear differential equation

$$\begin{aligned} \dot{r}^N(t) &= - \left[A^N - \left(B^N R^{-1} (B^N)^T - \frac{1}{\gamma^2} D^N (D^N)^T \right) \Pi^N \right]^T r^N(t) + \Pi^N F^N(t), \\ r^N(0) &= r^N(\tau). \end{aligned}$$

5.3 Machine Specifications

As one might well expect, the desired weighting for the design components of the \mathcal{D} operator is intimately related to the numerical stability of the solutions to the two Riccati equations in (5.2). From extensive studies on the numerical behavior of the condition numbers of the two Riccati solutions, it was observed that these solutions (condition numbers) depended heavily on the weighting of the matrices D^N , Q^N , R^N , and \mathcal{N}^N and the parameter γ . Acceptable condition numbers for Π^N were $\sim 10^{16}$ and for Σ^N were $\sim 10^{17}$. These were actually the best (smallest) condition numbers achieved with any weighting of the four matrices. Our preliminary calculations were performed on an IBM RISCSystem/6000 250 using double precision arithmetic. We point out that although the above condition numbers lie at the limits of double precision arithmetic, extensive numerical tests indicated consistent results and acceptable relative errors in the Riccati solutions. Moreover, good control results were obtained with these solutions. Hence we did not appear to be losing significant information in spite of the large condition numbers for the Riccati solutions. The weights in the matrices Q^N and R^N were actually not altered so as to provide a means of comparison with the results in [2], [6] and [8] where the same weights were used.

6 Numerical Results

We report here on a number of examples, each of which had been used in earlier calculations [2], [6] to test an LQR full state feedback methodology. For our computational tests here and in [2], [6], we chose physical parameters based on our experimental efforts reported elsewhere.

The parameter choices $a = 0.6 \text{ m}$, $l = 1 \text{ m}$, $\rho_f = 1.21 \text{ kg/m}^3$, $c^2 = 117649 \text{ m}^2/\text{sec}^2$, $\rho_b = 1.35 \text{ kg/m}$, $EI = 73.96 \text{ N} \cdot \text{m}^2$, $c_{DI} = 0.001 \text{ kg} \cdot \text{m}^3/\text{sec}$, $\mathcal{K}^B = 0.002331 \text{ N} \cdot \text{m}/V$ are reasonable for a .6 m by 1 m cavity with a thin beam at one end. The beam is assumed to have width and thickness .1 m and 0.005 m, respectively. The quadratic cost functional parameters were taken to be $R = 10^{-6}$ and $d_1 = d_2 = d_4 = 1$ and $d_3 = 1 \times 10^4$, with d_3 much larger than d_1, d_2 or d_4 in order to penalize large pressure variations (see also [2] for a discussion of the weights of \mathcal{Q} and R). The soft constrained differential game parameter γ was taken to be $\gamma = 1$.

For a simple set of runs, we used 6 cavity basis functions and 7 beam basis functions. Therefore $m = 48$ and $n = 8$ thus giving $N = 55$. The dimension of the overall system (both plant and state observer) in first order form is $4N$. Because the solutions are roughly periodic with period τ , the problems were solved as initial value problems with starting values $x^N(0) = 0$ and $r^N(t_f) = 0$ rather than as free boundary value problems. (Note that the final time t_f is chosen to be commensurate with the period τ).

Even though the numerical results obtained here are very encouraging, it is important to note that the solutions to the two Riccati equations are sensitive to the choice of the parameter γ and the weight in the operators $\mathcal{Q}, \mathcal{C}, \mathcal{D}$ and \mathcal{N} . The condition number for both Riccati solutions is affected by both the choice of γ and the weighting of the operators. As it was already mentioned in Section 5.3, an acceptable condition number for Σ is $\sim 10^{17}$ and for Π is $\sim 10^{16}$. Some of the examples presented in [2] and [6] are repeated here in the context of the H^∞ controller. The first, Example 6.1, whose open loop and state feedback solutions were presented in [6] as Example 4.2 and in [2] as Example 2 in the context of an LQR control methodology, is studied here utilizing the H^∞ theory mentioned above. The next example, Example 6.2, which is the same as Example 6.1 but with different initial conditions, illustrates the effects of the initial conditions on the compensator. Example 6.3, which was also studied in [6] as Example 4.3, exhibits the effect of multiple resonant excitation by an appropriately chosen forcing function f (see [6] for details). Off-resonant excitation is considered in Example 6.4 (initial LQR results for this example can be found in Example 4.4 of [6]). Continuing with the next example (Example 6.5) that uses the same information as Example 6.4, the effect of the number and location of microphones on the performance of the compensator is studied. We include as part of this last example a summary of findings on computations in which the pressure level at different points inside the cavity was tested using only a three microphone configuration for pressure measurements.

6.1 Example 1 - Resonant Excitation I

In this example (compare with Example 2 of [2]) we consider the system of Section 2 with the external force given by $f(t, \zeta) = 2.04 \sin(150\pi t)$ which models a periodic exterior plane wave with root mean square (rms) sound pressure level of 117 dB. Control was implemented via a pair of centered piezoceramic patches covering 1/6 of the beam.

The initial conditions given in terms of the vectors $\phi_0^N, w_0^N, \phi_1^N, w_1^N$ for the plant and $\hat{\phi}_0^N, \hat{w}_0^N, \hat{\phi}_1^N, \hat{w}_1^N$ for the state estimator are taken to be

$$\begin{bmatrix} \phi_0^N \\ w_0^N \end{bmatrix} = \begin{bmatrix} 0 \\ 0 \end{bmatrix}, \quad \psi_1^N = \begin{bmatrix} \phi_1^N \\ w_1^N \end{bmatrix} = \begin{bmatrix} 0 \\ 0 \end{bmatrix},$$

and

$$\begin{bmatrix} \hat{\phi}_0^N \\ \hat{w}_0^N \end{bmatrix} = \begin{bmatrix} 5 \times 10^{-1}[\zeta^3 - 1.5a\zeta^2 + a^3/4][(\psi - l)^2 - l^2/3] \\ 2 \times 10^{-3}[2\zeta^2 + 2(\zeta - a)^2 + 8\zeta(\zeta - a)] \end{bmatrix},$$

$$\begin{bmatrix} \hat{\phi}_1^N \\ \hat{w}_1^N \end{bmatrix} = \begin{bmatrix} 2 \times 10^0[\zeta^2(\zeta - a)^2 - a^4/30][(\psi - l)^2 - l^3/3] \\ 1 \times 10^{-2}[\sin^2(2\pi\zeta/a) \cos(2\pi\zeta/a)] \end{bmatrix},$$

where again, a is the length of the beam and l is the width of the cavity.

The sound pressure level at the point $(\zeta, \psi) = (0.30, 0.10)$ for the open loop, state feedback controlled and output feedback controlled approximate pressures for different levels of disturbance are presented in Table 6.1 for the time interval $[t_0, t_f] = [0, 10/75]$, and in Table 6.2 for the time interval $[3/75, 10/75]$. The root mean square pressures over a time interval, $[t_0, t_f]$, were calculated using the formula

$$p_{[t_0, t_f]}^{rms} = 20 \log \left(\frac{\sqrt{\frac{1}{(t_f - t_0)} \int_{t_0}^{t_f} p(t)^2 dt}}{2.04 \times 10^{-5}} \right) \text{ dB} \approx 20 \log \left(\frac{\sqrt{\frac{1}{N_{t_f}} \sum_{i=1}^{N_{t_f}} p(t_i)^2}}{2.04 \times 10^{-5}} \right) \text{ dB}.$$

(rms) Sound Pressure Level at $(\zeta, \psi) = (.3, .1)$ - (dB)			
% disturbance	Open Loop	State Feedback	Output Feedback
0	94.52	74.84	82.08
1	94.54	74.94	82.16
2	94.56	75.07	82.25
5	94.62	75.55	82.55
10	94.75	76.59	83.16

Table 6.1: Time interval [0,10/75].

From these tables one can see that the output feedback rms pressure is midway between those of the open loop and the full state feedback. The typical dB reduction is about 6 dB for all levels of disturbance, with the reduction improving when calculated on the interval $[3/75, 10/75]$.

(rms) Sound Pressure Level at $(\zeta, \psi)=(.3,.1)$ - (dB)			
% disturbance	Open Loop	State Feedback	Output Feedback
0	94.84	74.96	78.56
1	94.85	75.05	78.67
2	94.86	75.15	78.79
5	94.90	76.86	79.25
10	94.99	75.56	80.22

Table 6.2: Time interval [3/75,10/75].

The improvement seen in Table 6.2 when compared to Table 6.1 can be attributed to the fact that the compensator has an initial learning period before converging to the state of the plant. The time trajectory of pressure at $c_2 = (0.30, 0.10)$ for 0% and 5% disturbance level is shown in Figure 3 for the uncontrolled case, and the state and output feedback cases. The controlled cases use full state feedback controller and a controller based on the state estimator (the state observer uses 11 sensors/microphones: 3 displacement and 3 velocity sensors placed at $\zeta = 0.1, 0.3, 0.5$ and 5 microphones placed at points p_1, \dots, p_5 , as shown in Figure 2).

By comparing the results of Figure 3 (and Figure 6 of [6]) we can see that even with a 5% disturbance the compensator does perform satisfactorily. One should keep in mind that even though the full state feedback performs somewhat better than the output feedback (but both perform much better than the open loop case), the compensator does not require full information on the plant(which is not implementable) but rather 11 measurements of the beam velocity and displacement and the cavity pressure.

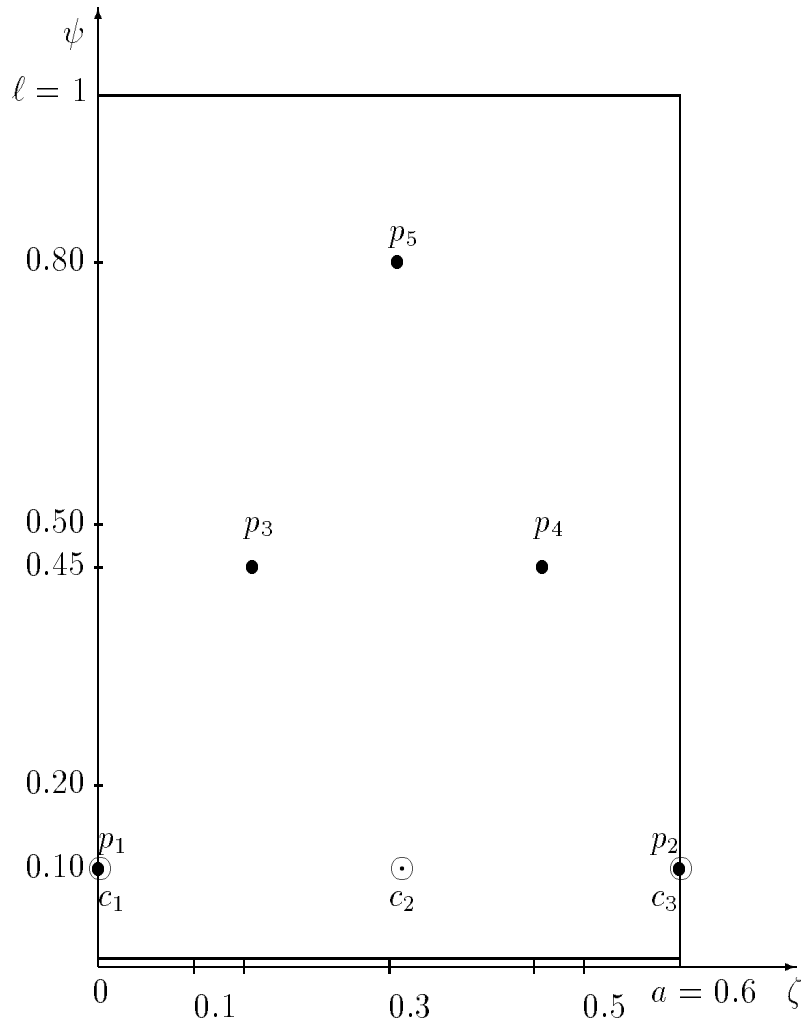
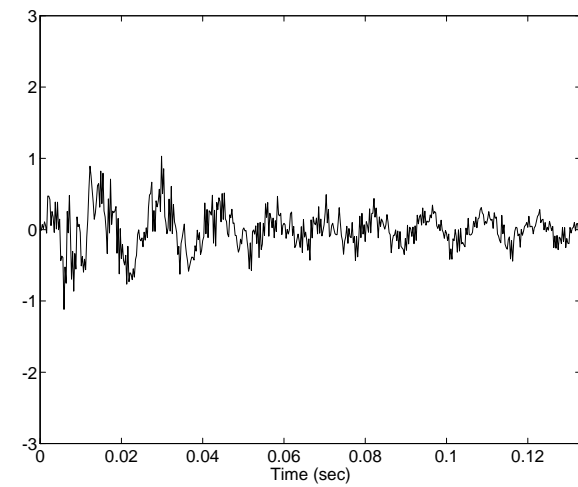
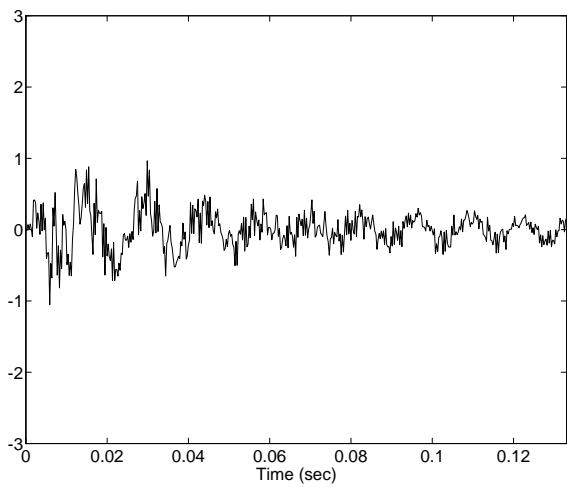
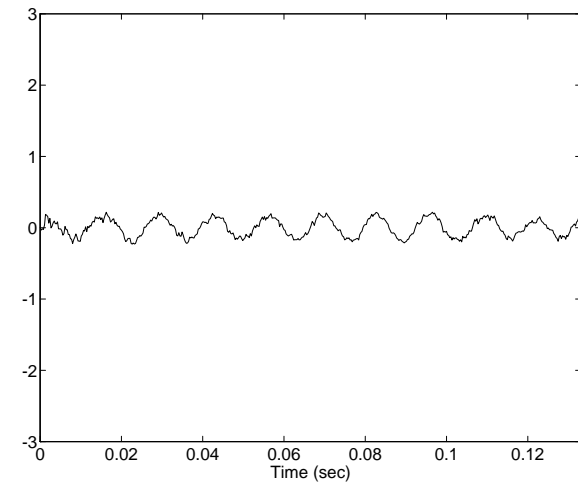
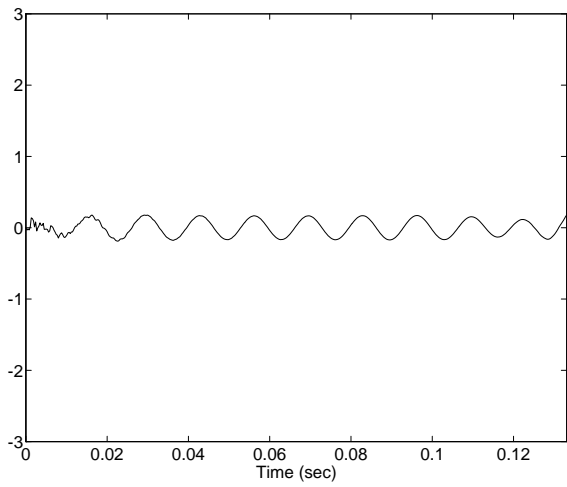
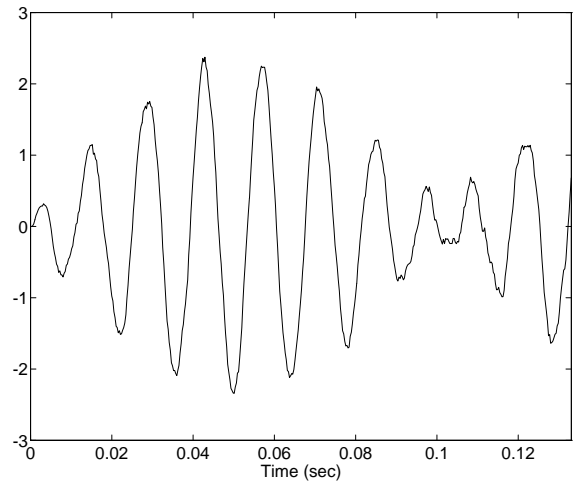
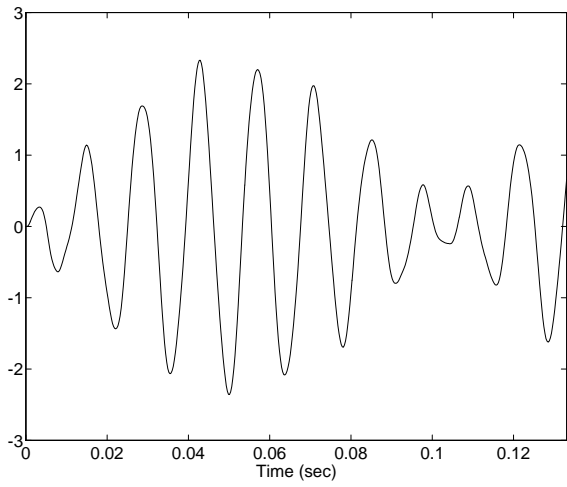


Figure 2: Sensor and microphone orientation in cavity - Sensors: $c_1=(0.00,0.10)$, $c_2=(0.30,0.10)$, $c_3=(0.60,0.10)$; Microphones: $p_1=(0.00,0.10)$, $p_2=(0.60,0.10)$, $p_3=(0.15,0.45)$, $p_4=(0.45,0.45)$, $p_5=(0.30,0.80)$.



0% disturbance

5% disturbance

Figure 3: Example 1 - Open Loop, State & Output Feedback Pressure (in order from top to bottom) at $c_2=(.3,.1)$ with 0% and 5% disturbance.

6.2 Example 2 - Resonant Excitation II: Effects of Initial Conditions

As a second example, we tested the effect of the initial conditions of the state estimator, $\hat{\phi}_0^N, \hat{w}_0^N, \hat{\phi}_1^N, \hat{w}_1^N$, on the performance of the controller. These are now taken to be a tenth of the previous values, namely

$$\begin{bmatrix} \hat{\phi}_0^N \\ \hat{w}_0^N \end{bmatrix} = \begin{bmatrix} 5 \times 10^{-2}[\zeta^3 - 1.5a\zeta^2 + a^3/4][(\psi - l)^2 - l^2/3] \\ 2 \times 10^{-4}[2\zeta^2 + 2(\zeta - a)^2 + 8\zeta(\zeta - a)] \end{bmatrix},$$

$$\begin{bmatrix} \hat{\phi}_1^N \\ \hat{w}_1^N \end{bmatrix} = \begin{bmatrix} 2 \times 10^{-1}[\zeta^2(\zeta - a)^2 - a^4/30][(\psi - l)^2 - l^2/3] \\ 1 \times 10^{-3}[\sin^2(2\pi\zeta/a) \cos(2\pi\zeta/a)] \end{bmatrix}.$$

Table 6.3 is the analogue of Table 6.1, where only the rms pressure of the compensator is given; values given in this table exhibit a significant difference in the reduction of the pressure level. In comparing the results of Tables 6.1 and 6.3, it can be seen that in the latter case, the performance of the compensator is close to that of full state feedback for low levels ($\leq 5\%$) of disturbance but weaker at the 10% disturbance level. Thus the initial conditions of the state estimator do affect the performance of the controller significantly. The time trajectory of the pressure (open loop, state feedback and output feedback) at the point $c_2 = (0.30, 0.10)$ for a 5% disturbance is shown in Figure 4. By comparing Figures 4 and 3 we see that the compensator's performance is much improved for a 5% disturbance level which also illustrates the substantial effects of the initial conditions.

Sound Pressure Level at $(\zeta, \psi)=(.3,.1)$ - (dB)	
% disturbance	Output Feedback
0	75.24
1	75.43
2	75.65
5	76.48
10	78.08

Table 6.3: Time interval [0,10/75].

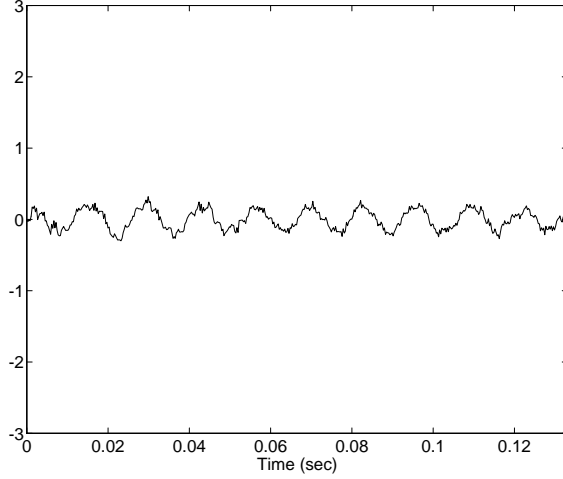


Figure 4: Example 2 - Output Feedback Pressure at (.3,.1) with 5% disturbance.

To provide additional insight on the effect of initial conditions, we switched the initial conditions in this example. That is, we assigned the nonzero initial conditions to the system (plant) and assumed zero initial conditions for the state estimator; hence

$$\begin{bmatrix} \phi_0^N \\ w_0^N \end{bmatrix} = \begin{bmatrix} 5 \times 10^{-2}[\zeta^3 - 1.5a\zeta^2 + a^3/4][(\psi - l)^2 - l^2/3] \\ 2 \times 10^{-4}[2\zeta^2 + 2(\zeta - a)^2 + 8\zeta(\zeta - a)] \end{bmatrix},$$

$$\begin{bmatrix} \phi_1^N \\ w_1^N \end{bmatrix} = \begin{bmatrix} 2 \times 10^{-1}[\zeta^2(\zeta - a)^2 - a^4/30][(\psi - l)^2 - l^2/3] \\ 1 \times 10^{-3}[\sin^2(2\pi\zeta/a) \cos(2\pi\zeta/a)] \end{bmatrix}.$$

and

$$\begin{bmatrix} \hat{\phi}_0^N \\ \hat{w}_0^N \end{bmatrix} = \begin{bmatrix} 0 \\ 0 \end{bmatrix}, \quad \begin{bmatrix} \hat{\phi}_1^N \\ \hat{w}_1^N \end{bmatrix} = \begin{bmatrix} 0 \\ 0 \end{bmatrix}.$$

The results (for the interval $[0, 10/75]$) in this case are given in Table 6.4. This shows no significant changes in the pressure level (for up to a 5% disturbance level) which illustrates that the switching of the initial conditions does not affect the full compensator performance. This suggests that it is the difference between the initial conditions of the plant (usually unknown to us) and those for the compensator (which we choose) that affect the performance of the compensator.

Sound Pressure Level at $(\zeta, \psi)=(.3,.1)$ - (dB)	
% disturbance	Output Feedback
0	74.60
1	74.75
2	74.95
5	75.76
10	77.44

Table 6.4: Time interval $[0,10/75]$.

6.3 Example 3 - Multiple Resonant Excitation

The forcing function in this example is given by

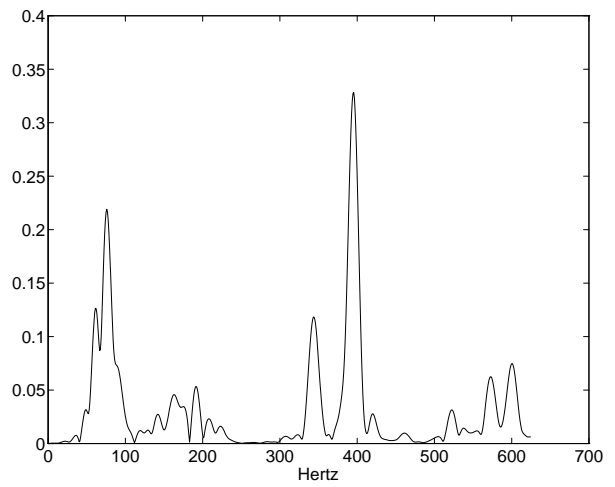
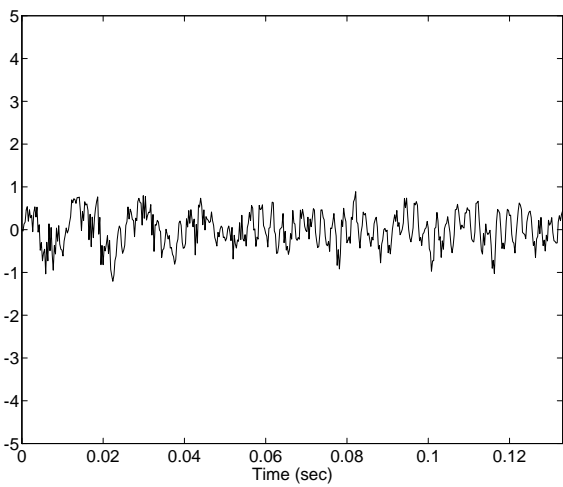
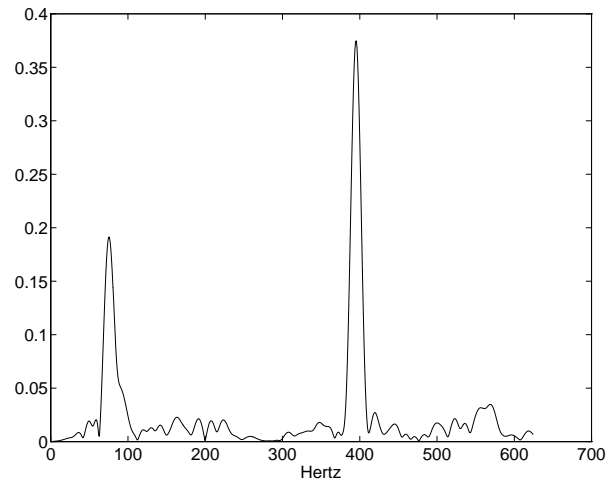
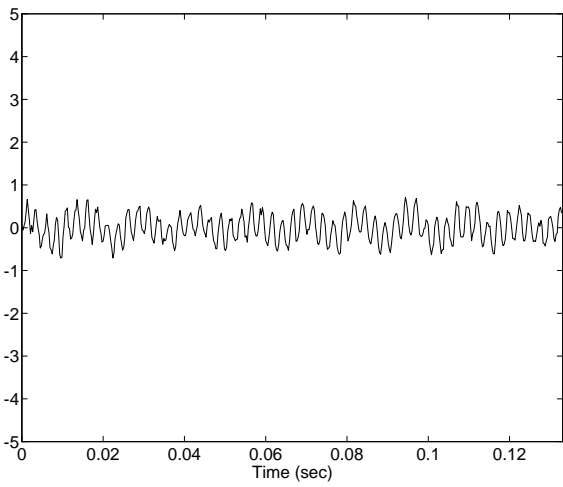
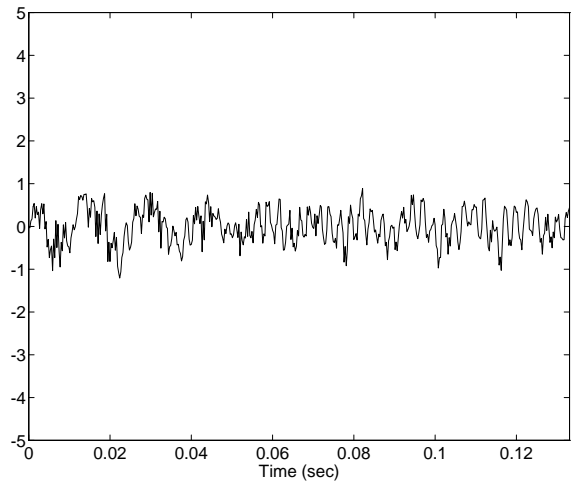
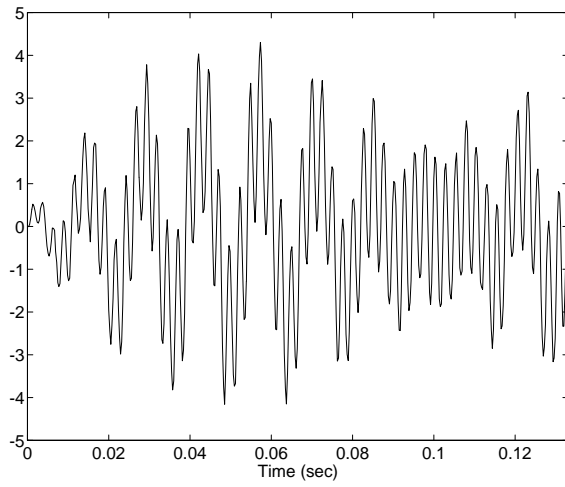
$$f(t, \zeta) = 2.04[\sin(150\pi t) + \sin(790\pi t)]$$

which excites the first and fourth system modes (see [6]), with natural frequencies at 65.9 and 387.7 hertz, respectively. This models a periodic plane wave with a sound pressure of 120 dB. As in the previous two examples, the control was implemented via a single pair of centered piezoceramic patch covering 1/6 of the beam length. The initial conditions for the state estimator are the same as those in Example 6.1.

The sound pressure level at the point $(\zeta, \psi) = (0.30, 0.10)$ for the uncontrolled, state feedback and output feedback controlled approximate pressures for different levels of disturbance are presented in Table 6.5 for the time interval $[3/75, 10/75]$. In this case the performance of the compensator is quite comparable to the performance of the full state controller. The time trajectories of the pressure at $(0.30, 0.10)$ (open loop, full state feedback and output state feedback) for a 5% disturbance level are shown in Figure 5(a), while the corresponding frequency responses are plotted on Figure 5(b). The cavity frequencies for the output feedback case reveal that the compensator captures the dominant frequencies but it also excites some other higher frequencies. This effect can be attributed to the high level of disturbance to which the compensator is responding.

(rms) Sound Pressure Level at $(\zeta, \psi)=(.3,.1)$ - (dB)			
% disturbance	Open Loop	State Feedback	Output Feedback
0	98.49	83.18	83.94
1	98.52	83.22	83.98
5	98.67	83.72	84.73

Table 6.5: Time interval $[3/75, 10/75]$.



(a) Cavity

(b) Cavity

Figure 5: Example 3 - Open Loop, State & Output Feedback Pressure at $(.3,.1)$ with 5% disturbance: (a) Time history (b) Frequency response (note differences in scales).

6.4 Example 4 - Off-Resonant Excitation

In this example the forcing function was taken to be $f(t, \zeta) = 2.04 \sin(470\pi t)$ with a frequency of 235 hertz which is approximately halfway between the natural frequencies of the first and fourth system modes. This models a periodic plane wave with an rms sound pressure level of 117 dB. Control in this example was implemented via a single centered pair of piezoceramic patches covering 1/2 of the beam length (see also Example 4.4 of [6]). The initial conditions for the compensator were taken to be the same as in Example 6.2, namely 1/10 of the initial conditions for Example 6.1. The sound pressure level at the point $(\zeta, \psi) = (0.30, 0.10)$ for the uncontrolled, state feedback and output feedback controlled approximate pressures for different levels of disturbance are presented in Table 6.6 for the time interval $[3/75, 10/75]$. This shows the remarkable performance of the compensator which closely resembles the performance of the full state feedback.

(rms) Sound Pressure Level at $(\zeta, \psi)=(.3,.1)$ - (dB)			
% disturbance	Open Loop	State Feedback	Output Feedback
0	82.55	70.07	70.26
1	82.56	70.05	70.27
5	82.64	70.15	70.58

Table 6.6: Time interval $[3/75, 10/75]$.

The time trajectories of the pressure at $(0.30, 0.10)$ (open loop, full state feedback and output state feedback) for 5% disturbance are shown in Figure 6. The frequencies of the uncontrolled and controlled (full state and output feedback) beam displacement (at 0.30) and cavity pressures (at $(0.30, 0.10)$) are plotted in Figure 7 for a 5% disturbance level. As it was also observed in Example 6.3, the compensator captures the dominant frequencies but also excites some other higher frequencies. We point out that in calculating the uncontrolled and controlled trajectories, we again used $n = 8$ beam and $m = 48$ cavity basis functions to discretize the problem. This is a smaller number than was used in Example 4.4 of [6] and some of the high frequency dynamics in the controlled cases may be slightly under-resolved. However, for purposes of comparison between the open loop, full state feedback and output state feedback results in this and previous examples, these limits suffice.

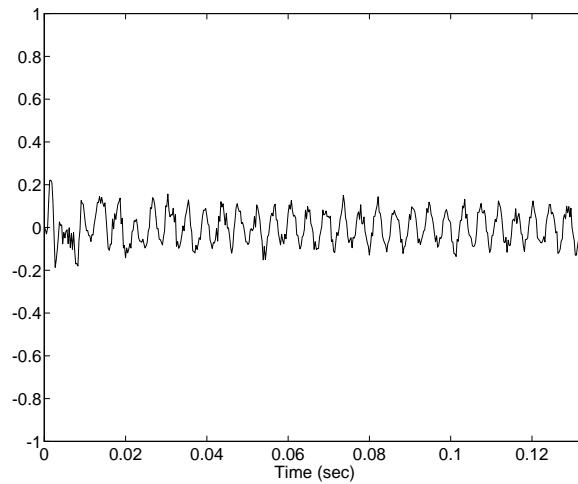
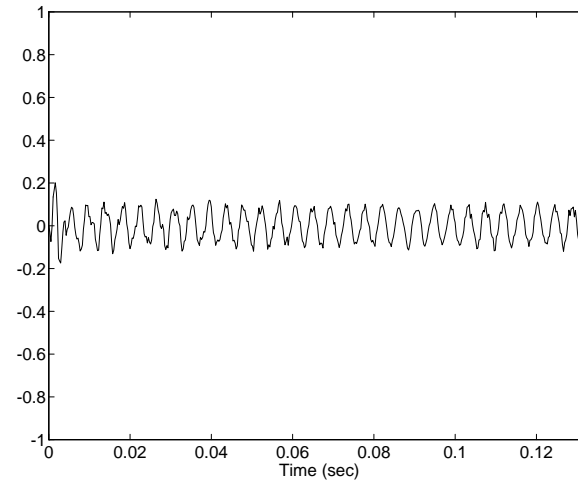
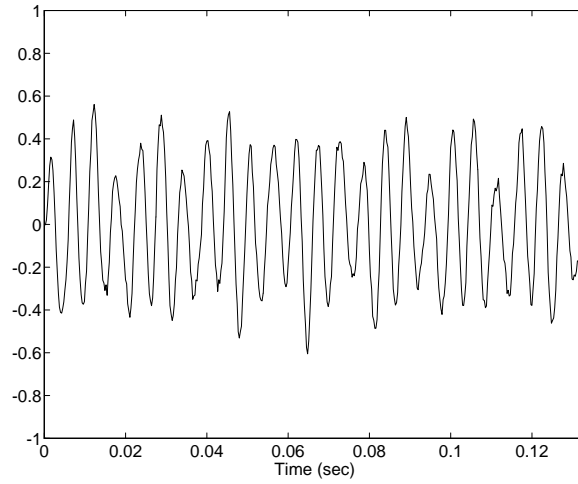
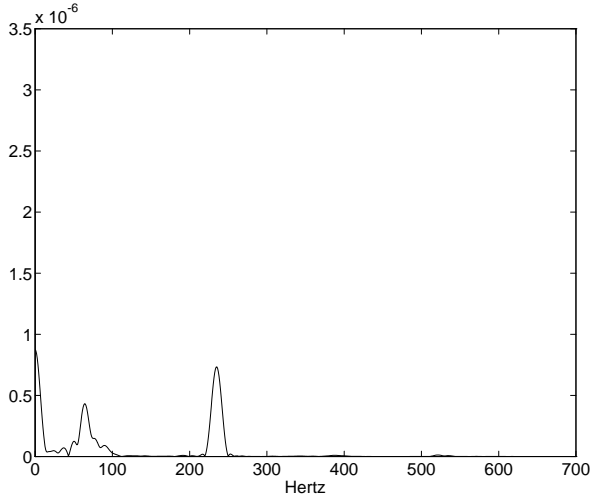
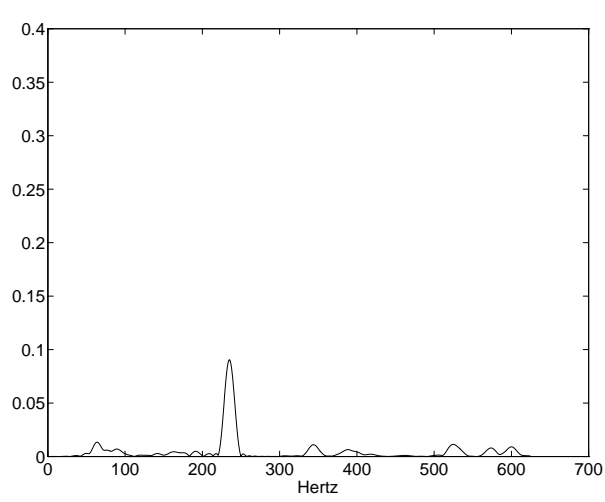
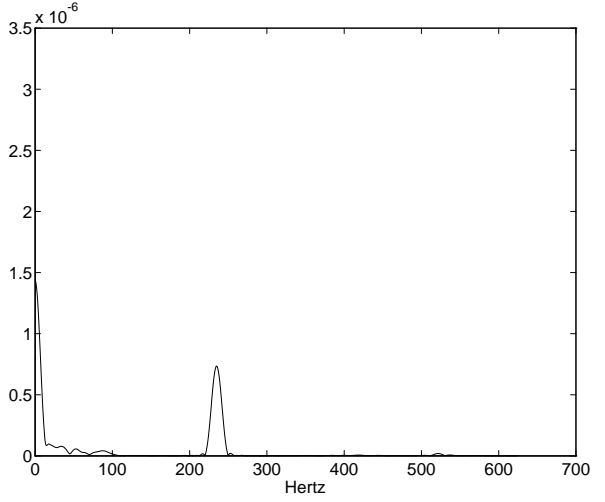
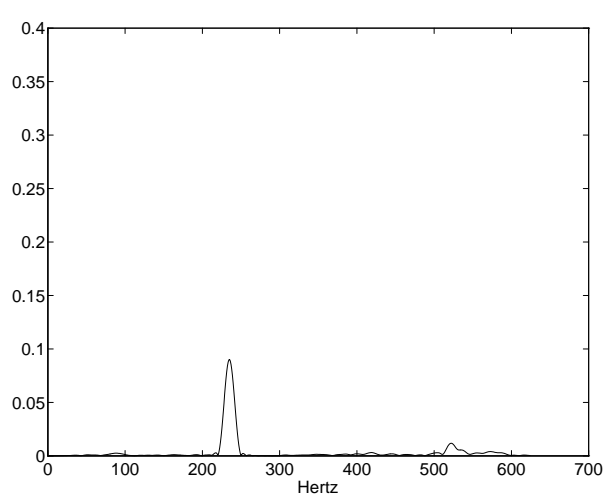
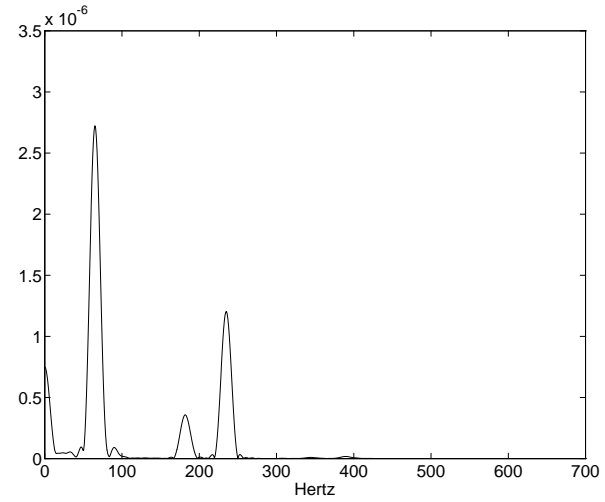
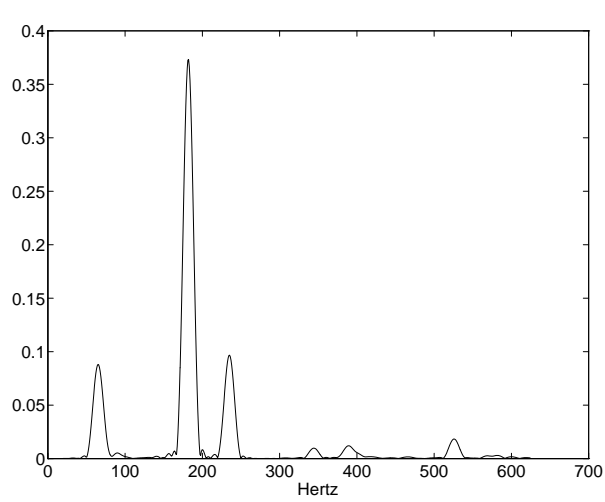


Figure 6: Example 4 - Open Loop, State & Output Feedback Pressure at (.3,.1) with 5% disturbance.



(a) Cavity

(b) Beam

Figure 7: Example 4 - Cavity and Beam Frequencies: Open Loop, State & Output Feedback for 5% disturbance.

6.5 Example 5 - Off-Resonant Excitation: Effects of microphones

We next consider the effects of microphone configuration on the performance of the MinMax compensator. The output feedback controller was tested for three different choices for the number of microphones, namely three, one, and finally no microphones at all, while the three displacement and three velocity sensors were kept fixed to provide information about the beam. The no microphone case is an important paradigm for the study of suppression of structure borne external cavity noise (such as for submarines and torpedos) where cavity microphones are not feasible. We used the same forcing function as in the previous example, $f(t, \zeta) = 2.04 \sin(470\pi t)$. The control was again implemented via a piezoceramic patch that covers half the length of the beam and $n = 8$ beam and $m = 48$ cavity basis functions were used in the approximate solutions. The initial conditions are the same as in the previous example.

The sound pressure level at the point $(\zeta, \psi) = (0.30, 0.10)$ for different choices of microphones, placed at the points p_1, p_2, p_5 and p_1 for the three and one microphone cases respectively, and for different levels of disturbance in the time interval $[3/75, 10/75]$ are given in Table 6.7. In this table the results from the previous example (i.e. open loop, state feedback and output feedback with five microphones) were added for comparison. It can be observed that the zero microphone case is comparable to the three and one microphone cases. In the computations using no microphone, the conditioning of the Riccati solution Σ was beyond the acceptable range. To alleviate this difficulty, one “fictitious” microphone was inserted at the point $(0, 0)$ in order to improve the conditioning but no readings from this microphone were used in the feedback. Finally, we note that the time trajectories of the pressure at the point $(0.30, 0.10)$ for 3, 1 or 0 microphones do not differ substantially from that with 5 microphones depicted in Figure 6.

(rms) Sound Pressure Level at $(\zeta, \psi)=(.3,.1)$ - (dB)						
disturbance %	Open Loop	State Feedback	Output Feedback Control			
			5 mic's	3 mic's	1 mic's	0 mic's(*)
0	82.55	70.07	70.26	70.29	76.05	79.29
1	82.56	70.05	70.27	70.29	76.09	79.36
5	82.64	70.15	70.58	70.62	76.30	79.68

Table 6.7: Time interval $[3/75, 10/75]$.

An additional study was undertaken to study the effects of the microphone location in the one microphone case (with three displacement and three velocity sensors again providing information about the beam). In these computations the microphone was placed in 30 different locations inside, or on the boundaries of, the cavity. In Table 6.8 we see how the orientation of the single microphone acting as the only pressure sensor would affect the performance of the compensator. As a first result we noticed that the condition number of the observer Riccati solution, Σ , varied from close to the acceptable range (i.e. $\sim 4.0 \times 10^{17}$) to the unacceptable case of $\sim 1.1 \times 10^{33}$. Another numerical effect is that the spectral radius of $\Pi\Sigma$ ranged from just below the prescribed bound $\gamma^2 = 1$ to the unstable value of $\sim 1.62 \times 10^{11}$. In addition to these numerical effects, the orientation also affected the

pressure levels which range from 73.99 dB (compared to 82.55 dB for open loop) to the completely unstable case of unbounded dB level.

Single microphone with 0% disturbance-Pres. at (.3,.1)			
location	sp. radius	cond(Σ)	pressure
(0.0,0.1)	0.935053e0	3.633523e17	76.06
(0.1,0.1)	1.408894e0	3.171438e18	75.44
(0.3,0.1)	9.152702e3	1.285535e23	70.39
(0.5,0.1)	1.408894e0	2.949970e18	75.72
(0.6,0.1)	0.935053e0	3.932790e17	76.14
(0.0,0.2)	1.197547e0	5.434848e17	78.77
(0.1,0.2)	1.751052e0	5.123897e17	78.50
(0.3,0.2)	1.736748e5	1.403098e23	∞
(0.5,0.2)	2.952413e0	5.304016e17	78.43
(0.6,0.2)	1.197547e0	5.429335e17	78.73
(0.0,0.5)	9.352854e0	6.601234e25	∞
(0.1,0.5)	1.588254e0	4.135351e17	78.91
(0.3,0.5)	2.288248e4	1.119943e33	∞
(0.5,0.5)	2.842567e7	5.239725e24	∞
(0.6,0.5)	5.710940e0	1.584858e21	∞
(0.0,0.8)	0.874731e0	5.103002e17	76.70
(0.1,0.8)	1.340855e0	4.883704e17	77.02
(0.3,0.8)	7.031469e4	1.370889e25	∞
(0.5,0.8)	2.984225e0	5.002226e17	77.90
(0.6,0.8)	0.874731e0	5.122637e17	77.04
(0.0,0.9)	0.783345e0	4.149297e18	75.65
(0.1,0.9)	2.211256e0	4.065758e17	76.47
(0.3,0.9)	5.375883e3	1.862700e24	∞
(0.5,0.9)	5.700614e0	4.089006e17	77.63
(0.6,0.9)	1.625439e11	5.326492e24	∞
(0.0,1.0)	0.772842e0	4.991717e17	73.99
(0.1,1.0)	1.173013e1	9.883714e18	74.13
(0.3,1.0)	9.234209e3	1.837065e25	∞
(0.5,1.0)	1.173013e1	8.008453e18	74.01
(0.6,1.0)	0.772842e0	5.138068e17	74.20

Table 6.8: Effects of microphone orientation.

In evaluating the effect of location in the single microphone case, it is noted that for this example, the best results appear to be obtained with a microphone placed on the cavity walls. Moreover, one notes good performance with a microphone placed either near the beam or near the back of the cavity with marked decrease in performance seen when the

microphone is located at the central points $(0.00, 0.50)$ and $(0.60, 0.50)$. This latter result is partially due the nature of the forcing function in this example. The 235 hertz driving force strongly excites the 181.6 hertz system mode which corresponds to the first mode for a cavity of this size with Neumann boundary conditions (as discussed in [6], the system modes differ slightly from the isolated beam and cavity modes due to the coupling between the two as well as damping in the beam). This mode has its strongest responses at the front and back of the cavity with a nodal line near the center. Hence a microphone located on the cavity walls near the center would be expected to have less effect than one located near the beam or close to the back wall. For different driving frequencies which excite different system modes, this result concerning microphone location may vary.

Furthermore, the observation that the optimal location for the microphone is along the boundary appears to be related to the numerical conditioning of the observer Riccati solution in this example (the effects of conditioning are also manifested in the slight non-symmetries appearing in the solutions). While demonstrating the feasibility of reducing the number of microphones to perhaps just one on the cavity boundary, the results in this example also demonstrate the need for further study regarding the effects and reduction of conditioning in the Riccati solutions.

Finally, the effects that various values of γ have on the spectral radius, the condition numbers of Π and Σ , and on the pressure level at the point $c_2 = (0.30, 0.10)$ are summarized in Table 6.9.

One microphone case at $(0.0, 1.0)$ with 0% disturbance					
value of γ	value of γ^2	sp. radius	cond(Π)	cond(Σ)	pressure
0.5000	0.250000	0.384845e0	1.454651e17	5.057469e17	96.50
0.9000	0.810000	0.279705e0	1.989576e16	5.080706e17	84.88
0.9990	0.008001	0.627114e0	1.529419e17	4.992364e17	71.12
1.0000	1.000000	0.772842e0	9.359363e16	4.991717e17	73.99
1.0100	1.020100	3.776310e0	8.181086e19	4.985420e17	72.86
1.1000	1.210000	0.177231e0	4.287271e17	2.801892e17	71.39
2.0000	4.000000	2.472911e1	1.116644e23	4.312765e17	87.72
5.0000	25.00000	4.125743e0	6.326601e18	4.277137e17	72.64
7.0000	49.00000	0.9440082	2.890659e16	4.273927e17	71.08
10.000	100.0000	1.351599e2	2.929152e18	4.272231e17	76.80
100.00	10000.00	1.284651e1	2.672224e16	4.276624e17	71.08
∞	∞	1.777402e1	2.061894e16	4.270608e17	71.08

Table 6.9: Effects of the value of γ .

For these results the point $(0.00, 1.00)$ (which provides an optimal single microphone location for this example), was used for the pressure measurements. The condition number for Σ appears to be proportional to the value of γ with reasonable pressure levels being obtained with $\gamma \geq 0.999$, whereas the condition number for Π does not exhibit such a proportionality but with acceptable pressure levels for again the same range of γ , namely $\gamma \geq 0.999$. Of course, with a different scaling of \mathcal{C} , \mathcal{D} , \mathcal{E} and \mathcal{Q} we can achieve the acceptable conditioning of Π and Σ for different (lower) values of γ . The measured pressured level at

the point $(0.30, 0.10)$ for the interval $[3/75, 10/75]$ and a 0% disturbance produces acceptable results for $\gamma \geq 1.00$. The range of γ for acceptable pressure levels can again be lowered by the proper scaling of \mathcal{C} , \mathcal{D} , \mathcal{E} and \mathcal{Q} . Such a study is not the current scope of our investigation, but will be undertaken in the future and reported on elsewhere. The limiting value $\gamma = \infty$, which is the standard Kalman filter, gives both acceptable condition numbers and pressure levels. This is no surprise since in these calculations the disturbance level is 0%.

From these studies one can conclude that the compensator can perform satisfactorily as compared to the full state feedback but that the location of microphones affects substantially its performance. A direct factor is the numerical instability that enters in the solution of the Riccati equations. One way to alleviate such a negative factor is to implement a numerically robust Riccati solver in which the number and location of microphones has less effect on the condition number and spectral radius. These simulations suggest the need of future investigation involving an in-depth study of the effects of the location and number of microphones (0 to 5 microphones) on the numerical conditioning and performance of the compensator.

In a continuation of this example, we also tested the compensator for pressure reduction at points other than the point $c_2 = (0.30, 0.10)$. We considered the pressure reduction at the five points, $(0.30, 0.20)$, $(0.50, 0.10)$, $(0.50, 0.30)$, $(0.50, 0.50)$, and $(0.30, 0.80)$ using three microphones placed at $(0.00, 0.10)$, $(0.30, 0.10)$ and $(0.60, 0.10)$ (points c_i , $i = 1, 2, 3$, in Figure 2) to provide information for the compensator. We used the same forcing function, patch length, and initial conditions as above. In these results some points have similar pressure level (dB) for both the full state and output feedback cases whereas some other points had some differences but both were still far below the open loop case. We found that the compensator pressure level checked at points other than the point $(0.30, 0.10)$ is frequently comparable to that of the full state feedback. This reinforces the conclusion that a compensator can perform almost as well as the full state feedback without the need of numerous sensors (compare with the 0 microphone case above). Another interesting conclusion is that if a number of microphones are to be used, they can in many cases be placed on the cavity walls or near the beam (a much easier and realizable configuration), as opposed to microphones placed in the central region of the cavity.

7 Concluding Remarks

This note represents a significant extension of earlier studies on the active control of a 2-D structural acoustic model with piezoceramic actuators. Our findings suggest that output feedback with a compensator/state estimator can produce significant control in a structure/acoustic cavity setting. As was demonstrated in the above examples the controller not only performs comparably to the full state controller but also maintains a degree of robustness (given by the H^∞ closed loop disturbance-to-performance output transfer function, having a bound γ). The conclusions of Example 6.5 are encouraging especially when a 3-D structural acoustic model is to be considered in which cavity microphones are not feasible. The implementation of a compensator that only requires pressure information from sensors placed on the walls of the cavity, will simplify both the construction and numerical and experimental implementation of such a controller.

A number of important factors in development of a control system such as that studied

here can be discerned from our studies reported above. First our studies suggest that the performance of the compensator can be significantly influenced by the choices of the initial conditions used for the state estimator systems. Other important considerations include the number, location, and type of sensors, the choice of approximation (order) in the computed gains, and the choice of design parameters which balance robustness of the control system versus stability of the computational algorithms.

ACKNOWLEDGEMENTS The authors are grateful to R.J. Silcox, Acoustics Division, NASA Langley Research Center, for numerous technical discussions and continued encouragement in our efforts on control of structure borne noise.

References

- [1] T. BAŞAR AND P. BERNHARD, *H[∞]-Optimal Control and Related Minimax Design Problems*, Birkhäuser, Boston-Basel-Berlin, 1991.
- [2] H. T. BANKS, W. FANG, R. J. SILCOX, AND R. C. SMITH, *Approximation methods for control of structural acoustics models with piezoceramic actuators*, Journal of Intelligent Material Systems and Structures, 4 (1993), pp. 98–116.
- [3] H. T. BANKS AND K. ITO, *A unified framework for approximation and inverse problems for distributed parameter systems*, Control-Theory and Advanced Technology, 4 (1988), pp. 73–90.
- [4] ———, *Approximation in LQR problems for infinite dimensional systems with unbounded input operators*, in SIAM Conference on Control in the 90's, San Francisco, 1989, preprint.
- [5] H. T. BANKS, K. ITO, AND Y. WANG, *Well posedness for damped second order systems with unbounded input operators*, Tech. Report 93-10, Center for Research in Scientific Computation, North Carolina State University, Raleigh, NC 27695, June, 1993; Differential and Integral Equations, submitted.
- [6] H. T. BANKS, R. J. SILCOX, AND R. C. SMITH, *The modeling and control of acoustic/structure interaction problems via piezoceramic actuators: 2-d numerical examples*, in ICASE Report No. 92-17, NASA Langley Research Center, Hampton, VA, April 1992, ASME Journal of Vibration and Acoustics, to appear.
- [7] H. T. BANKS AND R. C. SMITH, *Modelling and approximation of a coupled 3-d structural acoustics problem*, in Computation and Control III: Proceedings of the Third Boseman Conference, K. Bowers and J. Lund, eds., Birkhäuser, Boston-Basel-Berlin, 1993, pp. 29–48.
- [8] ———, *Feedback control of noise in a 2-d nonlinear structural acoustics model*, CRSC Report 93-14, Center for Research in Scientific Computation, North Carolina State University, Raleigh, NC 27695-8205, August, 1993; Control-Theory and Advanced Technology, submitted.
- [9] ———, *Models for control in smart material structures*, CRSC Report 92-21, Center for Research in Scientific Computation, North Carolina State University, Raleigh, NC

- 27695-8205, December, 1992; in *Identification and Control in Systems Governed by Partial Differential Equations*, SIAM, Philadelphia, 1993, pp. 26-44.
- [10] H. T. BANKS, Y. WANG, D. J. INMAN, AND J. C. SLATER, *Approximation and parameter identification for damped second order systems with unbounded input operators*, CRSC Report 93-9, Center for Research in Scientific Computation, North Carolina State University, Raleigh, NC 27695-8205, May, 1993; *Control: Theory and Advanced Technology*, to appear.
- [11] V. BARBU, *H_∞ boundary control with state feedback: the hyperbolic case*, in *Optimization, Optimal Control and Partial Differential Equations: First Franco-Romanian Conference*, Iasi, V. Barbu, J. F. Bonnans, and D. Tiba, eds., vol. 107 of International Series in Numerical Mathematics, Birkhäuser, Basel-Boston-Berlin, September 7-11 1992, pp. 141-148.
- [12] A. BENSOUSSAN AND P. BERNHARD, *Remarks on the theory of robust control*, in *Optimization, Optimal Control and Partial Differential Equations: First Franco-Romanian Conference*, Iasi, V. Barbu, J. F. Bonnans, and D. Tiba, eds., vol. 107 of International Series in Numerical Mathematics, Birkhäuser, Basel-Boston-Berlin, September 7-11 1992, pp. 149-166.
- [13] J. A. BURNS AND H. MARREKCHI, *Optimal fixed-finite dimensional compensator for burgers' equation with unbounded input/output operators*, in *Computation and Control III: Proceedings of the Third Boseman Conference*, K. Bowers and J. Lund, eds., Birkhäuser, Boston-Basel-Berlin, 1993, pp. 83-104.
- [14] R. H. FABIANO, A. J. KURDILA, AND T. STRGANAC, *Robust control of distributed parameter systems with structured uncertainty*, in *Computation and Control III: Proceedings of the Third Boseman Conference*, K. Bowers and J. Lund, eds., Birkhäuser, Boston-Basel-Berlin, 1993, pp. 193-201.
- [15] K. ITO, *Finite-dimensional compensators for infinite dimensional systems via galerkin-type approximation*, *SIAM Journal Control and Optimization*, 28 (1990), pp. 1251-1269.
- [16] B. V. KEULEN, *H_∞ -Control for Distributed Parameter Systems: A State-Space Approach*, Birkhäuser, Boston-Basel-Berlin, 1993.
- [17] ———, *The H_∞ -problem with measurement feedback for linear infinite dimensional systems*, *Journal of Mathematical Systems, Estimation, and Control*, (to appear).
- [18] B. V. KEULEN, M. PETERS, AND R. CURTAIN, *H_∞ control with state feedback: The infinite-dimensional case*, *Journal of Mathematical Systems, Estimation, and Control*, 3 (1993), pp. 1-39.
- [19] A. J. KURDILA, R. FABIANO, C. KIM, AND S. HSU, *Convergence of robust control design for distributed parameter systems*, in *AAS/AIAA Spaceflight Mechanics Meeting*, Colorado Springs, Colorado, February 24-26 1992.
- [20] A. J. KURDILA, R. FABIANO, T. STRGANAC, AND S. HSU, *Semigroup approximation and robust stabilization of distributed parameter systems*, in *Proceedings of The NASA Workshop on Distributed Parameter Modeling and Control of Flexible Aerospace Systems*, NASA Langley Research Center, Hampton, VA, June 8-9 1992.

- [21] I. LASIECKA, *Finite element approximations of compensator design for analytic generators with fully unbounded controls/observations*, SIAM Journal on Control and Optimization, (1994).
- [22] H. MARREKCHI, *Dynamic Compensators for a Nonlinear Conservation Law*, PhD thesis, Department of Mathematics, Virginia Polytechnic Institute and State University, Blacksburg, Virginia, September 1993.
- [23] P. M. MORSE AND K. U. INGARD, *Theoretical Acoustics*, Princeton University Press, Princeton, 1986.
- [24] I. RHEE AND J. L. SPEYER, *A game theoretic controller and its relationship to h_∞ and linear-gaussian synthesis*, in Proceedings of the 28th Conference on Decision and Control, Tampa, Florida, December 1989.
- [25] ———, *A game theoretic approach to a finite-time disturbance attenuation problem*, IEEE Trans. on Automatic Control, 36 (1991).